OXFORD GENETICS

GENETICS, 2024, 226(2), iyad196
https://doi.org/10.1093/genetics/iyad196
Advance Access Publication Date: 9 November 2023
Investigation

The SWI/SNF nucleosome remodeler constrains enhancer activity during *Drosophila* wing development

Matthew J. Niederhuber [1,2,3,4], Mary Leatham-Jensen,[2,3,4] Daniel J. McKay [2,3,4,*]

[1]Curriculum in Genetics and Molecular Biology, The University of North Carolina at Chapel Hill, Chapel Hill, NC 27599, USA
[2]Department of Biology, The University of North Carolina at Chapel Hill, Chapel Hill, NC 27599, USA
[3]Department of Genetics, The University of North Carolina at Chapel Hill, Chapel Hill, NC 27599, USA
[4]Integrative Program for Biological and Genome Sciences, The University of North Carolina at Chapel Hill, Chapel Hill, NC 27599, USA

*Corresponding author: Department of Biology, Department of Genetics, Integrative Program for Biological and Genome Sciences, The University of North Carolina at Chapel Hill, Chapel Hill, 250 Bell Tower Drive, 3358 Genome Sciences Building, NC 27599-7100, USA. Email: dmckay1@email.unc.edu

Chromatin remodeling is central to the dynamic changes in gene expression that drive cell fate determination. During development, the sets of enhancers that are accessible for use change globally as cells transition between stages. While transcription factors and nucleosome remodelers are known to work together to control enhancer accessibility, it is unclear how the short stretches of DNA that they individually unmask yield the kilobase-sized accessible regions characteristic of active enhancers. Here, we performed a genetic screen to investigate the role of nucleosome remodelers in control of dynamic enhancer activity. We find that the *Drosophila* Switch/Sucrose Non-Fermenting complex, BAP, is required for repression of a temporally dynamic enhancer, br^{disc}. Contrary to expectations, we find that the BAP-specific subunit Osa is dispensable for mediating changes in chromatin accessibility between the early and late stages of wing development. Instead, we find that Osa is required to constrain the levels of br^{disc} activity when the enhancer is normally active. Genome-wide profiling reveals that Osa directly binds br^{disc} as well as thousands of other developmentally dynamic regulatory sites, including multiple genes encoding components and targets of the Notch signaling pathway. Transgenic reporter analyses demonstrate that Osa is required for activation and for constraint of different sets of target enhancers in the same cells. Moreover, Osa loss results in hyperactivation of the Notch ligand Delta and development of ectopic sensory structures patterned by Notch signaling early in development. Together, these findings indicate that proper constraint of enhancer activity is necessary for regulation of dose-dependent developmental events.

Keywords: nucleosome remodeler; chromatin; enhancer; developmental gene regulation

Introduction

Animal development requires robust control over the spatial patterns, magnitude, and temporal dynamics of gene expression. Dysregulation in any of these regulatory dimensions is known to contribute to developmental disorders and acquired disease states. Spatial control refers to the selective patterns of gene expression across a field of cells. For instance, the spatially restricted expression of Hox genes in animals is essential for the specification of regional identities along the developing body axis (Mallo and Alonso 2013). Both loss of expression and ectopic expression of Hox genes beyond their normal spatial domains can lead to homeotic transformations. The magnitude of gene expression must also be tightly controlled for proper development, and both excessive and insufficient gene expression can be detrimental. For instance, duplication of the *APP* gene is associated with early-onset Alzheimer's disease and is thought to be a driver of Alzheimer's in individuals with Trisomy 21 (Tang and Amon 2013). Conversely, heterozygosity of Notch pathway components, including the Notch receptor itself, is associated with several developmental syndromes (Falo-Sanjuan and Bray 2020). This dose dependency is conserved in *Drosophila*, which exhibits defects in sensory organ development when genes encoding Notch pathway components are mutated, as well as in genotypes with extra copies of Notch pathway genes (Hartenstein and Posakony 1990; Parks and Muskavitch 1993; Doherty *et al.* 1996; Elfring *et al.* 1998; Armstrong *et al.* 2005). The spatial patterns and levels of gene expression are also temporally dynamic, as cells transition through intermediate identities over developmental time. A classic example of temporal regulation is ecdysone hormone signaling in insects, which triggers changes in stage-specific gene expression programs across body parts that are not in close physical contact (Yamanaka *et al.* 2013). Despite their importance, the factors and mechanisms coordinating these 3 dimensions of developmental gene regulation remain incompletely understood.

A primary layer of gene regulation lies at the level of *cis*-acting DNA regulatory elements and the *trans*-acting factors that bind them. Enhancers are relatively short (~0.5–2 kb) noncoding regions of DNA that function as integration points for the spatiotemporal information transmitted by sequence-specific transcription factors, which typically bind short DNA sequences 6–10 bp in length (Spitz and Furlong 2012; Uyehara and Apostolou 2023). Additional layers of information come in the form of the packaging and chemical modification of chromatin. Histone posttranslational modifications directly and indirectly control chromatin structure and help propagate cellular memory

Received on 05 October 2023; accepted on 30 October 2023

(Millán-Zambrano et al. 2022). Access to DNA-encoded information is also influenced by the positioning, stability, and occupancy of nucleosomes. Nucleosomes are inhibitory to transcription factor binding and thus must be remodeled or removed for an enhancer to become active (Brahma and Henikoff 2020; Niederhuber and McKay 2021 ; Isbel et al. 2022). For this reason, genome-wide patterns of chromatin accessibility are predictive of enhancer activity. Moreover, temporal changes in chromatin accessibility profiles are correlated with stage-specific changes in gene expression during development (Uyehara et al. 2017). Recent studies in *Drosophila* have provided insight into the mechanisms controlling developmentally programmed changes in chromatin accessibility. A number of transcription factors have been identified that open chromatin in early-stage embryos to promote activation of the zygotic genome (Gaskill et al. 2021). Likewise, the ecdysone-induced transcription factor E93 has been found to be required for promoting the accessibility of enhancers active later in pupal stages of development (Nystrom et al. 2020). Interestingly, E93 is also necessary for closing and deactivating early-acting enhancers (Uyehara et al. 2017; Nystrom et al. 2020). Returning accessible enhancers to a closed chromatin state is important for rendering them refractory to transcription factor binding, thereby allowing regulatory inputs to be utilized at distinct targets over the course of development. However, the mechanisms of closing chromatin to repress enhancers during development are poorly understood relative to those controlling chromatin opening.

Here, we examine the contribution of nucleosome remodeling complexes in the control of developmentally dynamic enhancers in *Drosophila*. Nucleosome remodelers use ATP hydrolysis to disrupt histone–DNA interactions and, by doing so, occlude or make accessible short stretches of DNA to transcription factors. Through mechanisms that remain unclear, disruption of short stretches of histone–DNA contacts by nucleosome remodelers can result in the accessibility of enhancers that are often orders of magnitude greater in length (Clapier et al. 2017). Through an in vivo RNAi screen, we identified the *Drosophila* BAP complex, which is orthologous to yeast and human Switch/Sucrose Non-Fermenting (SWI/SNF), as being required for repression of a developmentally dynamic enhancer. Contrary to expectations, we find that BAP is dispensable for developmentally programmed changes in chromatin accessibility during wing metamorphosis. Instead, we find that the BAP subunit Osa is required to constrain activity when the enhancer is in the ON state. Using CUT&RUN, we find that Osa directly binds thousands of regions that have signatures of active enhancers, including multiple genes in the Notch signaling pathway. Transgenic reporter analyses demonstrate that Osa is required for the activation of some target enhancers while also being required for the constraint of other target enhancers in the same cells. Lastly, we find that loss of BAP function results in upregulation of a newly identified enhancer of the *Delta* gene, which encodes the Notch ligand, leading to *Delta* hyperactivation. Together, these data suggest a model in which the BAP complex directly constrains the activity of a subset of its target enhancers to ensure correctly measured responses to developmental signals like Notch signaling and cell specification programs during wing development.

Methods

Plasmid construction

The *br^{disc}-tdTomato-PEST* vector was made by cloning a PEST degradation tag from *w;20xUAS-FLPG5.PEST^{attP40}*; (Bloomington 55806), using previously published primers (Nern et al. 2011). The PEST sequence was inserted into the previously described pDEST-attR1/2-tdTomato by HiFi assembly (Uyehara et al. 2017). The *br^{disc}* enhancer was moved into the destination vector by Gateway cloning (Invitrogen). The reporter was integrated into the *attP2*, *VK33*, and *86FB* landing sites. The *br^{disc}-FRT-tdTomato-2xSTOP-FRT-myrGFP* (*br^{disc}-switch*) reporter was generated from pJFRC177 *10xUAS-FRT-2xSTOP-FRT-myrGFP* (Addgene 32149). The *br^{disc}* enhancer was restriction cloned into the *HindIII* and *AatII* sites, replacing the upstream UAS elements. *tdTomato* cDNA sequence was subsequently restriction cloned into the *NheI* site. The reporter was integrated into the *attP2* landing site. The *Dl^{pouch}* enhancer (dm6 chr3R: 19310086–19311243) was gateway cloned into the pFUGG GAL4 and the pDEST-attR1/2-tdTomato-PEST vectors and then integrated into the genome at attP2 and 86FB, respectively. Genomic insertions were made via PhiC31 integration. Injections were performed by BestGene or Genetivision.

Primers used are described in Table 1.

Drosophila culture and genetics

For *br^{disc}-switch* experiments, RNAi expression was driven by *en-GAL4, tub-GAL80$^{ts.10}$* driver. Crosses were raised at 23°C until being shifted to 29°C to induce RNAi. Animals were heat shocked at 37°C for 1 h to induce Flippase (FLP) expression under the control of the heat-inducible *hsFLP* promoter and then recovered at 29°C for several hours to allow expression of myristoylated GFP (myr-GFP) before dissection. For imaginal discs, crosses were moved to 29°C for 72–96 h after egg laying (AEL), and third larval wandering (3LW) animals were heat shocked 48 h later and then recovered for 4 h before dissection. For pupal wings, crosses were moved to 29°C for 96–120 h AEL, and prepupae [0–12 h after puparium formation (APF)] were staged using the absence of head eversion as a developmental marker, heat shocked 24 h later (24–36 h APF), and then recovered for either 4 h (28–40 h APF) or 6 h (30–42 h APF) for the older wing shown in Fig. 1b.

For RNAi screening using the *br^{disc}-tdTomato-PEST^{86Fb}* reporter, RNAi expression was driven by *ci-GAL4, UAS-GFP, tub-GAL80$^{ts.10}$* driver. Crosses were raised at 23°C until being shifted to 29°C to induce RNAi at 72–96 or 96–120 h AEL, depending on the severity of phenotypes with individual RNAi lines. Prepupae were staged as described above and then dissected 24 h later (24–36 h APF). The same protocol was followed (induction at 72–96 h AEL) to evaluate enhancer response to Osa knockdown in third larval wing imaginal discs. RNAi lines used in the screen are reported

Table 1. Primers used for plasmid construction.

tdTomato_NheI_Fwd	gaccatacgctagctttcgtttagccaagactcg
tdTomato_NheI_Rev	attctagggctagcagtgttgcatgtttcgaagg
br-disc_hindIII_Fwd	ggccgcaagcttgagtgtgtgcgagtgaatga
br-disc_AatII_Rev	gcgctcgacgtcccgaggaaagagcagaagatg
PEST_fwd	tgaagttgccctcgctagcCATGGCTTCCCTCCAGAG
PEST_rev	tgccgactggcttagttaattaattctagaTTACACGTTGATGCGAGC
Dl-pouch_Fwd	TTTTAGCACCCACTGACCGA
Dl-pouch_Rev	TACTGAAAATGGCCATCAAGTG

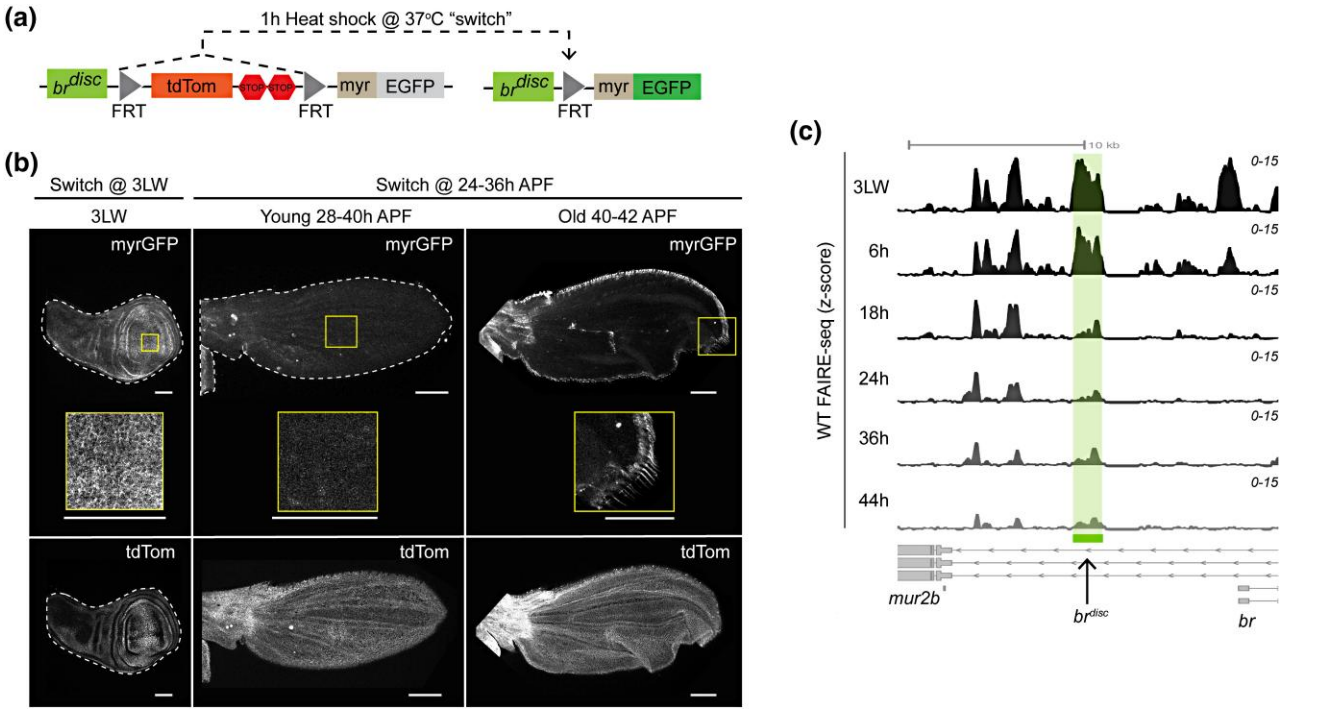

Fig. 1. The *br*^{disc} enhancer is a model of a developmentally dynamic regulatory element. a) Illustration of the *br*^{disc}*-switch* reporter. Heat shock-induced FLP expression excises the FRT-flanked "*tdTomato, 2xSTOP*" cassette to allow expression of myr-GFP. b) Confocal images of *br*^{disc}*-switch* activity in 3LW imaginal wing discs and pupal wings aged 28–42 h APF. "Young" and "old" denote pupal wings categorized by aging and morphology (see Methods for additional staging details). "Switch @" denotes ages of animals at the time of heat shock. Images of pupal wings are MIPs. Image of imaginal wing disc is single slice. Scale bars are 100 µm. Wings are shown with anterior up. c) Genome browser shot of z-normalized FAIRE-seq signal at the *br*^{disc} enhancer (highlighted) from time course of WT wing development.

in Supplementary Table 1. Additional RNAi lines used included *H* (Bloomington 27315 and 34703), *su(H)* (Bloomington 67928), *pan* (Bloomington 26743), *E93* (Bloomington 57868), and *luciferase* (Bloomington 31603).

For Osa-deGrad experiments, females of the genotype *UAS-Nslmb-vhhGFP4;osa*^{GFP}*/(TM6B, Tb)* were crossed to males with either *nub-GAL4, tub-GAL80*$^{ts.10}$*/CyO, Tb-RFP;osa*^{GFP}*/(TM6B, Tb)* or *osa*^{GFP}*/(TM6B, Tb)* for the negative control lacking GAL4. Crosses were raised at 23°C until 3LW stage. Larvae were moved to 29°C (Cho *et al.* 2020), prepupae were staged 12 h later, and non-Tubby female pupal wings were dissected 24 h later (24–36 h APF). For late Osa-deGrad immunofluorescence experiments, females with *en-GAL4, tub-GAL80*$^{ts.10}$*;osa*^{GFP}*/TM6B, Tb* were crossed to males with *UAS-Nslmb-vhhGFP4;br*^{disc}*-tdTomato-PEST*^{VK33}*, osa*^{GFP}*/TM6B, Tb*. Crosses were kept at 23°C until prepupal stage (0–12 h APF) and then moved to 29°C to induce degradation. Non-tubby pupae (*osa*^{GFP} homozygous) were dissected 30 h later (30–42 h APF). Tubby pupae (*osa*^{GFP} heterozygous) were used as a negative control. Younger wings (~28–38 h APF) were identified within the staged range of 28–40 h APF and by morphology (small size, absence of folding, and absence of elongated bristle shafts along the margin). Older wings (>40 h APF) were identified within the staged range of 30–42 h APF and by morphology (presence of folds, flattened/expanded cells in wing blade, and presence of elongated bristle shafts along the margin) (Sobala and Adler 2016; Diaz and Thompson 2017; Guild *et al.* 2005; Cho *et al.* 2020).

For *osa*^{308} mitotic clone experiments, males with the genotype *yw122;;br*^{disc}*-tdTomato-PEST*^{attP2}*, FRT82B, ubi-GFP/TM6B, Tb* were crossed to females with the genotype *yw;;FRT82B, osa*^{308}*/TM6B, Tb* at 23°C (day 0). On day 5, vials with larvae were heat shocked in a 37°C water bath for 20 min and then recovered at 25°C for 48 h; 0–12 h APF prepupae were staged (pre-head eversion) and aged for ~28 h before dissection. Wings were stained with mouse anti-Osa (1:200) and goat anti-mouse Alexa 633 (1:1,000).

For CUT&RUN, cultures were raised at 25°C.

Lines used are as follows:

- yw;en-GAL4, tub-GAL80$^{ts.10}$;br^{disc}-FRT-tdTomato-2xSTOP-FRT-myr-GFP^{attP2}/(TM6B, Tb)
- yw;ci-GAL4, UAS-GFP, tub-GAL80$^{ts.10}$/(CyO);br^{disc}-tdTomato-PEST ^{86Fb}/(TM6B, Tb)
- yw;ci-GAL4, UAS-GFP, tub-GAL80$^{ts.10}$/(CyO);br^{disc}-tdTomato-PEST ^{VK33}/(TM6B, Tb)
- yw;;Dl^{pouch}-tdTomato-PEST^{86FB}/(TM6B, Tb)
- yw;;Dl^{pouch}-GAL4^{attP2}
- yw;ci-GAL4, UAS-GFP, tub-GAL80$^{ts.10}$/(CyO);E74^{A}-tdTomato-PEST^{86FB}/(TM6B, Tb)
- yw;ci-GAL4, UAS-GFP, tub-GAL80$^{ts.10}$/(CyO);E74^{B}-tdTomato-PEST^{86FB}/(TM6B, Tb)
- yw;en-GAL4, tub-GAL80$^{ts.10}$;osa^{GFP}/(TM6B, Tb)
- yw;UAS-Nslmb-vhhGFP4;osa^{GFP}/(TM6B, Tb)
- w;nub-GAL4^{AC-62}, tub-GAL80$^{ts.10}$/CyO, Tb-RFP; osa^{GFP}/(TM6B, Tb)
- yw122;;UAS-osa-RNAi ^{attP2}/(TM6B) – (Derived Bloomington 31266)
- yw122;;UAS-lexA-RNAi ^{attP2}/(TM6B) – (Derived Bloomington 67945)
- yw;;osa^{GFP}/(TM6B, Tb) – (Derived Bloomington 51579)
- yw122;;br^{disc}-tdTomato-PEST ^{attP2}, FRT82B, ubi-GFP/TM6B, Tb
- yw;;FRT82B, osa^{308}/TM6B, Tb – (Bloomington 5949)

- yw;;

See Supplementary Table 1 for a complete list of RNAi lines used in screen.

See Supplementary Table 2 for a list of SWI/SNF subunits and corresponding RNAi lines tested. We used FlyBase (release FB2023_05) to find information on phenotypes/function/stocks/gene expression (etc) (Gramates *et al.* 2022).

Immunofluorescence and image analysis

Larvae and pupae were dissected as previously described (Uyehara *et al.* 2017). Primary antibodies are as follows: 1:100 mouse anti-Osa (Developmental Studies Hybridoma Bank [DSHB]), 1:100 rat anti-Elav (DSHB), and 1:10 mouse anti-Delta (DSHB). Secondary antibodies are as follows: goat anti-mouse Alexa-633, goat anti-mouse Alexa-647, and goat anti-rat Cy5 were used at 1:1,000 (Invitrogen). Tissue was mounted in VECTASHIELD (Vector Labs) with 1.5 coverslips.

For image quantification of RNAi screen microscopy, a custom Python script was used to compare reporter signal in RNAi-expressing vs wild-type (WT) cells in each wing. Briefly, 10–20 slice z-stacks were converted to maximum intensity projections (MIPs). Masks were generated of DAPI, GFP-positive RNAi-expressing, and DAPI–GFP (GFP-negative) non-RNAi-expressing regions. A ratio of mean gray values in GFP-positive and GFP-negative regions was calculated for each wing.

For image quantification of br^{disc} hyperactivation, Dl^{pouch} hyperactivation, and Delta immunofluorescence experiments, MIPs were made for each wing, and then regions were selected in RNAi-expressing and WT control cells of the imaginal disc pouch for each wing. For br^{disc} and Dl^{pouch} hyperactivation, square regions were selected that straddled the margin. For Delta quantification, regions were manually drawn around the margin from the anterior–posterior boundary to the approximate edge of the most distal provein, L2 in the anterior and L5 in the posterior. Mean gray values were measured using ImageJ (Schindelin *et al.* 2012), and a ratio of mean gray value in RNAi vs WT control was calculated. Student's two-sample *t*-tests were performed in R to calculate significance.

High throughput sequencing and data analysis

For FAIRE-seq, wings of female pupae were prepared as previously described (Uyehara *et al.* 2017; Uyehara and Mckay 2019). Forty wings were used per biological replicate. Libraries were prepared using the Takara ThruPLEX DNA-seq Kit with unique dual indexes following the manufacturer's specifications and sequenced on an Illumina NextSeq 2000. Adapters were trimmed from paired-end reads using BBmap BBDuk (v38.71) and then aligned to the dm6 *Drosophila* genome assembly with Bowtie 2 (v2.3.4.1; Langmead and Salzberg 2012) with the following parameters: –very-sensitive --no-unal --no-mixed --no-discordant --phred33 -I 10 -X 700. Aligned reads were filtered using an exclusion list for dm6 from ENCODE (Amemiya *et al.* 2019) and quality filtered ($q > 5$) with SAMtools (v1.9; Danecek *et al.* 2021), and duplicate reads were removed with Picard (v2.2.4). Coverage files were generated with deepTools (v2.4.1; Ramírez *et al.* 2016) and normalized to 1× genomic coverage (Reads Per Genome Coverage [RPGC]). Peaks were called with MACS2 (v2.1.2; Zhang *et al.* 2008) using standard parameters. z-normalized coverage files were generated with a custom R script (4.1.3) from RPGC normalized files. For visualization, biological replicates were pooled using SAMtools (v1.9). Differential peak analysis was performed in R using DiffBind (v3.8.4; Stark and Brown 2011) and DEseq2 (v1.38.3; Love *et al.* 2014). For the assignment of "Osa-dependent" peaks into "increasing," "decreasing," or "static" categories, each peak was annotated with z-normalized WT FAIRE-seq data from 3LW and 6, 18, 24, 36, and 44 h APF wings (Uyehara *et al.* 2017). A $\log_2$ ratio was calculated at each time point relative to 3LW. "Increasing" peaks were those that had a $\log_2$FoldChange ≥ 1 at 24, 36, or 44 h APF. "Static" peaks were those that had a $\log_2$FoldChange between -1 and 1 at 24, 36, and 44 h APF. "Decreasing" peaks were all remaining peaks. Later pupal stages (24, 36, and 44 h) were used for categorization because they corresponded with the approximate stage of wings used for Osa-deGrad FAIRE-seq. Pearson correlation heatmaps of z-normalized coverage files were generated using deepTools (3.5.1).

For WT FAIRE-seq time course, previously published raw data were accessed from Gene Expression Omnibus (GEO) GSE131981 (Ma *et al.* 2019). Data were aligned and processed as described above except alignment was run using Bowtie 2 with the --very-sensitive parameter and no additional changes.

For Osa-GFP CUT&RUN female wing, imaginal discs from either *yw;;*osa^{GFP} or *yw* negative control animals were dissected and processed as previously described (Uyehara and Mckay 2019); 20–22 wing discs were used for each replicate, with a rabbit anti-GFP (1:100, Rockland 600-401-2156), a pAG-MNase (1:100; UNC core; Salzler *et al.* 2023), and 0.5 ng of yeast genomic DNA spike-in (gift of Steve Henikoff). Libraries were prepared from the "supernatant" fraction using the Takara ThruPLEX DNA-seq Kit with unique dual indexes and following the manufacturer's specifications but with a modified amplification step as previously described (Uyehara and Mckay 2019). Libraries were pooled and sequenced on an Illumina NextSeq 2000 with a 75-bp read length. Adapters were trimmed from paired-end reads using BBmap BBDuk (v38.71) and then aligned to the dm6 *Drosophila* genome assembly with Bowtie 2 (v2.3.4.1) with the following parameters: --local --very-sensitive-local --no-unal --no-mixed --no-discordant --phred33 -I 10 -X 700. Aligned reads were filtered using a custom exclusion list generated from the "supernatant" of IgG negative controls, as well as anti-Flag and anti-GFP experiments in genotypes that lacked either the Flag or GFP epitopes. Peaks shared among all these negative controls were used to make a conservative list of reproducible high-signal regions. This exclusion list included ∼80 regions. Reads were then quality filtered ($q > 5$) with SAMtools (v1.10), and duplicate reads were removed with Picard (v2.2.4). Coverage files were generated with deepTools (v2.4.1) and normalized to 1× genomic coverage (RPGC). Peaks were called with MACS2 (v2.1.2) without a control and using the --nomodel and --nolambda parameters. z-normalized coverage files were generated with a custom R script (v4.1.3) from RPGC normalized files.

For H3 lysine 27 acetylation (H3K27ac) CUT&RUN, 20 male imaginal wing discs were used per replicate, with a rabbit anti-H3K27ac (1:100, Active Motif #39135). Libraries were prepared from the "pellet" fractions using the Takara ThruPLEX DNA-seq Kit as described above. Libraries were pooled and sequenced on an Illumina Novaseq SP with a 75-bp read length. Reads were aligned and processed as described above, except peaks were called with standard MACS2 settings and a sheared genomic DNA control.

For CUT&RUN analysis, only Osa-GFP peak calls greater than or equal to the 50th percentile of MACS2 quality scores (qval) that were identified in both replicates were kept. Osa peaks were identified as those that passed screens for quality and reproducibility but did not intersect a reproducible control peak. Peak annotation

was performed in R using the ChIPseeker package (v1.34.1; Yu *et al.* 2015), and a negative control bootstrapped shuffle of Osa peaks was generated using the nullranges package (v1.4.0; Mu *et al.* 2023). Peak overlap enrichment analysis for Hairless Chromatin Immunoprecipitation (ChIP) and rotund (Rn) ChIP-seq (Fig. 5g and j) was performed in R using ChIPseeker. Osa peaks were clustered by dynamic accessibility patterns (Fig. 5h) by annotating peaks with replicate pooled and z-normalized WT FAIRE-seq data at 3LW and 6, 18, 24, 36, and 44 h APF. For each peak, the fraction of max FAIRE signal was calculated for each time point. k-means clustering was performed in R with a *k* of 8, based on previously described 8 distinct clusters of FAIRE patterns using these data (Nystrom *et al.* 2020). Motif enrichment analysis was performed in R using the memes package (v1.6.0; Nystrom and McKay 2021) and the AME software (McLeay and Bailey 2010; Nystrom and Mckay 2021).

For Rn ChIP-seq, raw sequencing data were downloaded from the GEO database (GSE203208; Loker and Mann 2022). Rn ChIP-seq data were processed using snakePipes (v2.7.3; Bhardwaj *et al.* 2019). Reads were aligned to dm6 with Bowtie 2 (v2.4.5), and peaks were called with MACS2 (v2.2.7.1).

For Hairless ChIP-chip analysis, peak calls were downloaded from GEO (GSE97603; Chan *et al.* 2017).

All plots were generated in R using the ggplot2 package (v3.4.2; Wickham 2016), genome browser plots were generated with the Gviz package (v1.42.1; Hahne and Ivanek 2016), and heatmaps were generated with the CompexHeatmap package (v2.14.0; Gu *et al.* 2016)

Results

The br^{disc} enhancer is a model of a developmentally dynamic regulatory element

In order to interrogate the role of nucleosome remodelers in developmentally dynamic enhancer regulation, we selected a previously identified enhancer known to respond to temporal inputs from the ecdysone hormone pathway (Uyehara *et al.* 2017; Nystrom *et al.* 2020). The br^{disc} enhancer is a ~2-kb region on the X chromosome that lies ~9-kb upstream of the gene *broad* (*br*). Prior studies of br^{disc} activity using transgenic reporters indicated that it switches on prior to the third larval instar stage in the precursors of the adult appendages, including the wing (Uyehara *et al.* 2017). Br^{disc} is then deactivated during the first 24 h of pupal development, thus making it a good model for studying temporally dynamic enhancer control.

We first sought to improve the temporal resolution of br^{disc} transgenic reporter activity. Traditional enhancer reporters optimize rapid fluorophore maturation, brightness, and stability. Although these optimizations are useful for sensitive detection of enhancer activity patterns, they are problematic when monitoring dynamic enhancer behavior because persistent fluorescent protein interferes with determining when enhancer activity shuts off. To mitigate these effects, we developed 2 new fluorescent reporters. The first is a dual fluorophore reporter system, which we refer to as br^{disc}-*switch*. This reporter was designed to drive expression of a tandem tomato fluorophore (tdTomato) that could be inducibly switched via FLP/FRT-meditated recombination to transcribe a myr-GFP (Fig. 1a). The *switch* reporter system allows for better temporal resolution of enhancer dynamics relative to conventional reporters because GFP detected after reporter switching indicates the enhancer was transcriptionally active after recombination was induced. Conversely, a lack of GFP detected after reporter switching demonstrates that the enhancer was inactive at the time of recombination or later. Examination of br^{disc}-*switch* activity revealed that the reporter is highly active in 3LW wing imaginal discs, but there is little to no detectable nascent GFP in young pupal wings aged 28–40 h APF (Fig. 1b; Supplementary Fig. 1a). By contrast, tdTomato signal remains high in this same wing (Fig. 1b). Interestingly, the br^{disc}-*switch* reporter exhibits new GFP signal in older (40–42 h APF) wings, in bristle shafts located along the wing margin and in cells of the posterior cross vein, indicating that it is reactivated in a subset of pupal wing cells after its initial deactivation. Closer inspection of another transgenic br^{disc} reporter integrated at a separate genomic locus, and which employs a different minimal promoter, revealed similar late enhancer activity along the wing margin (Supplementary Fig. 1b). Thus, the observed spatiotemporal changes in reporter expression are likely driven by the enhancer rather than DNA sequences in the vector or surrounding genomic regions.

Comparison of temporal changes in br^{disc} reporter activity and a chromatin accessibility time course performed in developing WT wings revealed a strong correlation between reporter activity and endogenous enhancer accessibility. Br^{disc} exhibits high accessibility in 3LW wing discs, remains in an open state during the prepupal stage at 6 h APF, and subsequently loses most of its accessibility by 18 h APF, shortly after the prepupal to pupal transition (Uyehara *et al.* 2017; Fig. 1c). These accessibility profiles are congruent with changes in reporter activity. We note that the later reactivation of br^{disc} along the pupal wing margin does not coincide with a detectable increase in accessibility. This may be due to a lack of sensitivity to detect changes in a small number of cells using whole-wing FAIRE-seq. Alternatively, the small amount of accessibility that remains at later stages may derive from this population of cells. Together, these observations demonstrate that br^{disc} is dynamically active and accessible during wing development, thus making it a useful model for studying the mechanisms of dynamic enhancer regulation.

The *Drosophila* BAP nucleosome remodeling complex is required to repress br^{disc}

To identify factors that contribute to the developmental dynamics of br^{disc} enhancer activity during wing metamorphosis, we performed an in vivo RNAi screen. As described above, conventional fluorescent reporters are engineered to be highly stable, making them poorly suited for detecting changes in enhancer activity. While the *switch* reporter corrects this problem by using a 2-fluorophore output, it is too technically cumbersome for use in a larger-scale screen. To circumvent this limitation while optimizing screen throughput, we created a second new transgenic fluorescent reporter in which the br^{disc} enhancer drives tdTomato fused to a C-terminal PEST degradation tag (br^{disc}-*tdT-PEST*; Li *et al.* 1998; Nern *et al.* 2011). This design yielded increased sensitivity for detecting br^{disc} dysregulation, as determined by comparing reporter levels in the presence and absence of the PEST tag upon knockdown of a known br^{disc} repressor (Supplementary Fig. 2a). We interpret the increase in sensitivity to be due to increased tdTomato turnover relative to the nontagged version. Despite the addition of the PEST tag, a low but detectable level of tdTomato expression was observed in WT pupal wing cells, which we interpret as residual fluorophore expression from earlier times in development when the enhancer is active (Supplementary Fig. 2a). RNAi expression was controlled by the UAS/GAL4 system via the *cubitus interruptus* anterior compartment GAL4 driver (*ci-GAL4*). A ubiquitously expressed temperature-sensitive allele of the GAL4 repressor GAL80 (*tub-GAL80*^{ts}) was used to restrict

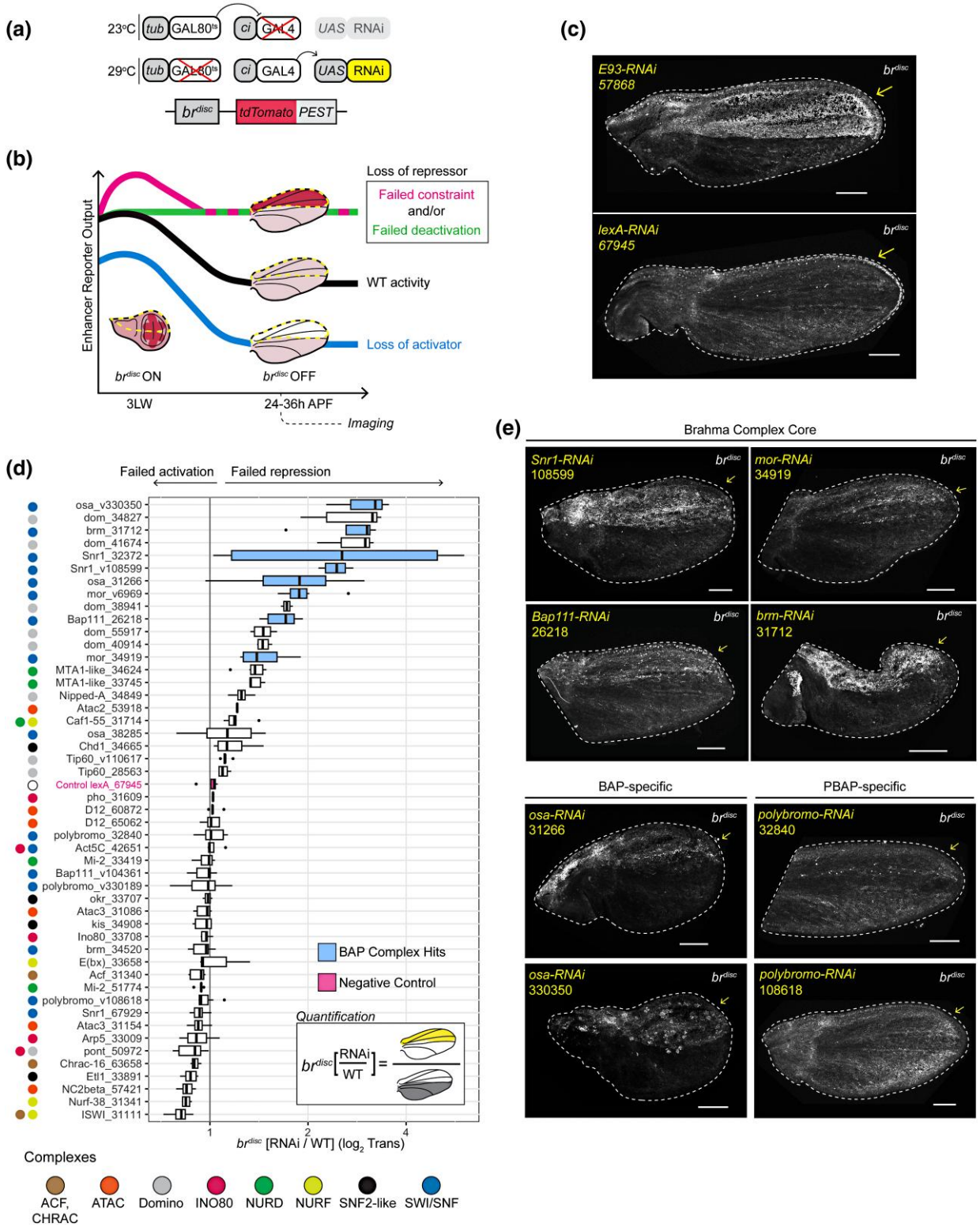

Fig. 2. The BAP complex is required to repress the br^{disc} enhancer. a) Illustration of the br^{disc}-*tdTomato-PEST* reporter and inducible RNAi system used to screen for genes required for br^{disc} regulation. b) Schematic of types of enhancer dysregulation detectable in the RNAi screen. RNAi-expressing cells are located within the yellow dashed outline. Temporal activity of reporter in WT cells is indicated by black line. Loss of an activator in 3LW imaginal wing discs (br^{disc} ON) would cause reduced reporter levels in RNAi cells (blue line). Failed deactivation (br^{disc} OFF) would cause increased levels of reporter activity in RNAi cells (green line). Failed constraint in wing discs (br^{disc} ON) would also cause increased levels in RNAi cells (magenta line). c) Confocal images of positive (*E93-RNAi*) and negative (*lexA-RNAi*) controls. Yellow arrows indicate regions of RNAi expression. Stock identification numbers are indicated (see Supplementary Table 1). d) Quantification of changes in br^{disc} reporter activity induced by RNAi. Boxplots summarize ratios of br^{disc} signal in RNAi cells to WT cells. Each data point is a different wing. Each RNAi line tested is plotted on the y-axis, with gene symbol followed by RNAi line ID; colored circles denote complex association. "v" preceding line number indicates VDRC. A negative control *lexA* RNAi (magenta) has a ratio of ~1. Subunits of the BAP complex are indicated in light blue. Inset illustration depicts method of quantification. x-axis is log2 transformed. e) Confocal images of br^{disc} activity after RNAi of select core components of the BAP complex. Images are maximum projections. Scale bars are 100 µm.

RNAi expression to later stages of development (ci^{ts}; Fig. 2a). We envisioned 2 potential outcomes upon RNAi knockdown of br^{disc} regulators: loss of an activator would yield decreased levels of tdTomato relative to control cells, and loss of a repressor would yield increased levels of tdTomato relative to control cells. We reasoned that by screening for tdTomato levels in pupal wings, we would potentially capture 2 types of repressors, those that deactivate br^{disc} over time and those that constrain the levels of br^{disc} activity while it is on in larval stages (Fig. 2b). Knockdown of the transcription factor Eip93F (E93), a known negative regulator of br^{disc} expressed during pupal stages, resulted in increased br^{disc} reporter activity in pupal wings, whereas expression of a negative control *lexA*-RNAi failed to impact br^{disc} activity, confirming the sensitivity of our reporter screen design to detect changes in enhancer activity (Fig. 2c).

We focused our RNAi screen on nucleosome remodelers, reasoning that the functions of these enzymatic complexes in controlling nucleosome occupancy, positioning, and stability may contribute to developmentally programmed changes in enhancer accessibility. We tested a total of 48 RNAi lines corresponding to 30 genes encoding components of major ATP-dependent nucleosome remodeling complexes and associated factors (Clapier *et al.* 2017; Supplementary Table 1). These include members of all 4 families of remodeling complexes: imitation switch (ISWI), SWI/SNF, chromodomain helicase DNA binding (CHD), and inositol requiring 80 (INO80). Specific *Drosophila* nucleosome remodeling complexes include members of the ATP-utilizing chromatin assembly and remodeling factor (ACF) and chromatin accessibility complex (CHRAC), the Ada-two-A-containing (ATAC) complex, the SWI/SNF Brahma Complex (BAP and PBAP), the domino complex, the INO80 complex, the nucleosome remodeling deacetylase (NuRD) complex, the nucleosome remodeling factor (NURF) complex, and several additional noncomplex-associated SNF2-like remodeler proteins (Supplementary Table 1). To summarize the results of the screen, we quantified the average intensity of the br^{disc} reporter in RNAi-expressing cells (anterior compartment), normalized to WT cells (posterior compartment) within the same wing (KD/WT; Fig. 2d). Two genes were identified that decreased reporter activity in pupal wings, including *Iswi*, which is a component of the ACF, CHRAC, and NURF remodeling complexes (Bouazoune and Brehm 2006; Supplementary Fig. 2c). Eight genes were identified that increased reporter activity (Fig. 2d; Supplementary Table 1). Remarkably, 5 of these 8 genes are subunits of the *Drosophila* SWI/SNF BAP complex. These include *osa*, *moira* (*mor*), *Snr1*, *Bap111*, and the core ATP-ase Brahma (*brm*). In some cases, we found that RNAi lines targeting the same gene gave divergent results in our screen. For instance, 2 independent RNAi lines for *Snr1* yielded some of the strongest increases in br^{disc} activity (lines 32372 and 108599) while a third line (67929) produced little change. Similarly, of the 2 RNAi lines targeting *brm*, only 1 (31712) had a significant effect on br^{disc} reporter activity. Notably, RNAi lines that significantly impacted reporter activity often caused lethality, with many animals dying as pupae or pharate adults (Supplementary Table 1). By contrast, the *brm* and *Snr1* RNAi lines that did not impact reporter activity had little to no impact on animal survival or wing development. Since both *brm* and *Snr1* are essential genes, we interpret the lack of phenotype caused by these RNAi lines to be a consequence of poor target knockdown. Due to the enrichment of Brahma complex members among hits, we chose to characterize the role for this nucleosome remodeler in br^{disc} repression. We did not pursue other hits further.

There are 2 distinct versions of the Brahma complex in *Drosophila*, BAP and PBAP, which are defined by the mutually exclusive association of either Osa (BAP), or Polybromo, SAYP, and Bap170 (PBAP; Cenik and Shilatifard 2021). We find that multiple RNAi lines targeting *osa* resulted in derepression of br^{disc} in the pupal wing, whereas 3 independent RNAi lines for *polybromo* had no effect on the normal dynamics of br^{disc} by either qualitative observation or image quantification (Fig. 2e; Supplementary Fig. 2d and Table 2). We did not observe significant lethality or dramatic changes in wing morphology with any of the tested *polybromo* RNAi lines, suggesting that either these *polybromo* RNAi reagents are ineffective in the context of our screen or Polybromo is not required for wing development at this stage. Although we cannot definitively exclude PBAP, the finding that Osa is required for br^{disc} reporter repression demonstrates a role for the Osa-specific BAP complex in the dynamic regulation of this enhancer. Homozygous *osa* mutant cells generated by mitotic recombination also exhibited increased br^{disc} reporter activity (Supplementary Fig. 2e), further supporting a role of Osa and the BAP complex in br^{disc} repression. Lastly, we reasoned that Osa loss-of-function experiments would result in fewer pleiotropic effects relative to the depletion of a core Brahma complex subunit. For these reasons, we focused on the Osa-specific BAP complex in subsequent experiments.

Osa is largely dispensable for pupal patterns of chromatin accessibility

Deactivation of temporally dynamic enhancers is associated with decreased chromatin accessibility over developmental time, and failure to deactivate temporally dynamic enhancers coincides with aberrantly persistent chromatin accessibility (Uyehara *et al.* 2017). Our observation that Osa depletion causes derepression of the br^{disc} reporter in pupal wings (Fig. 2e) raised the possibility that the BAP complex may be required for the closing of temporally dynamic enhancers. To test the genome-wide role of Osa in the developmental control of chromatin accessibility, we performed FAIRE-seq in an *osa* degradation genotype. We employed the GFP deGrad system in conjunction with a genotype, osa^{GFP}, in which both *osa* alleles are tagged with GFP (hereafter Osa-deGrad; Buszczak *et al.* 2007; Caussinus *et al.* 2012; Supplementary Fig. 3a). The GFP deGrad system enables target proteins to be more rapidly degraded than RNAi-based knockdown, which is especially important in pupal wings because they undergo few cell divisions following pupariation (Ma *et al.* 2019; Fig. 3a). Animals homozygous for osa^{GFP} are viable and do not exhibit any morphological or developmental defects, indicating that Osa-GFP protein is functional. Confocal microscopy of osa^{GFP} heterozygous imaginal wing discs showed nuclear-localized GFP that colocalized with endogenous Osa. Moreover, GFP signal was specifically depleted upon expression of *osa* RNAi, validating the identity of this genotype (Supplementary Fig. 3b). Osa-GFP degradation was induced in animals homozygous for osa^{GFP} during the late larval stage (3LW). Prepupal animals were staged (0–12 h APF) and aged for ~24 h before dissection such that total degradation time was ~36 h (Fig. 3a). Consistent with our RNAi results, we observed near-complete loss of Osa-GFP protein in the pupal wing blade under these conditions and a corresponding increase in br^{disc} reporter activity, demonstrating the efficacy of Osa-deGrad depletion (Fig. 3b). Immunofluorescence for Osa under these degradation conditions confirmed significantly reduced nuclear Osa signal relative to control (Supplementary Fig. 3c). Osa-deGrad flies that were permitted to develop longer exhibited reduced wing size and high rates of lethality, with most animals dying as pharate adults.

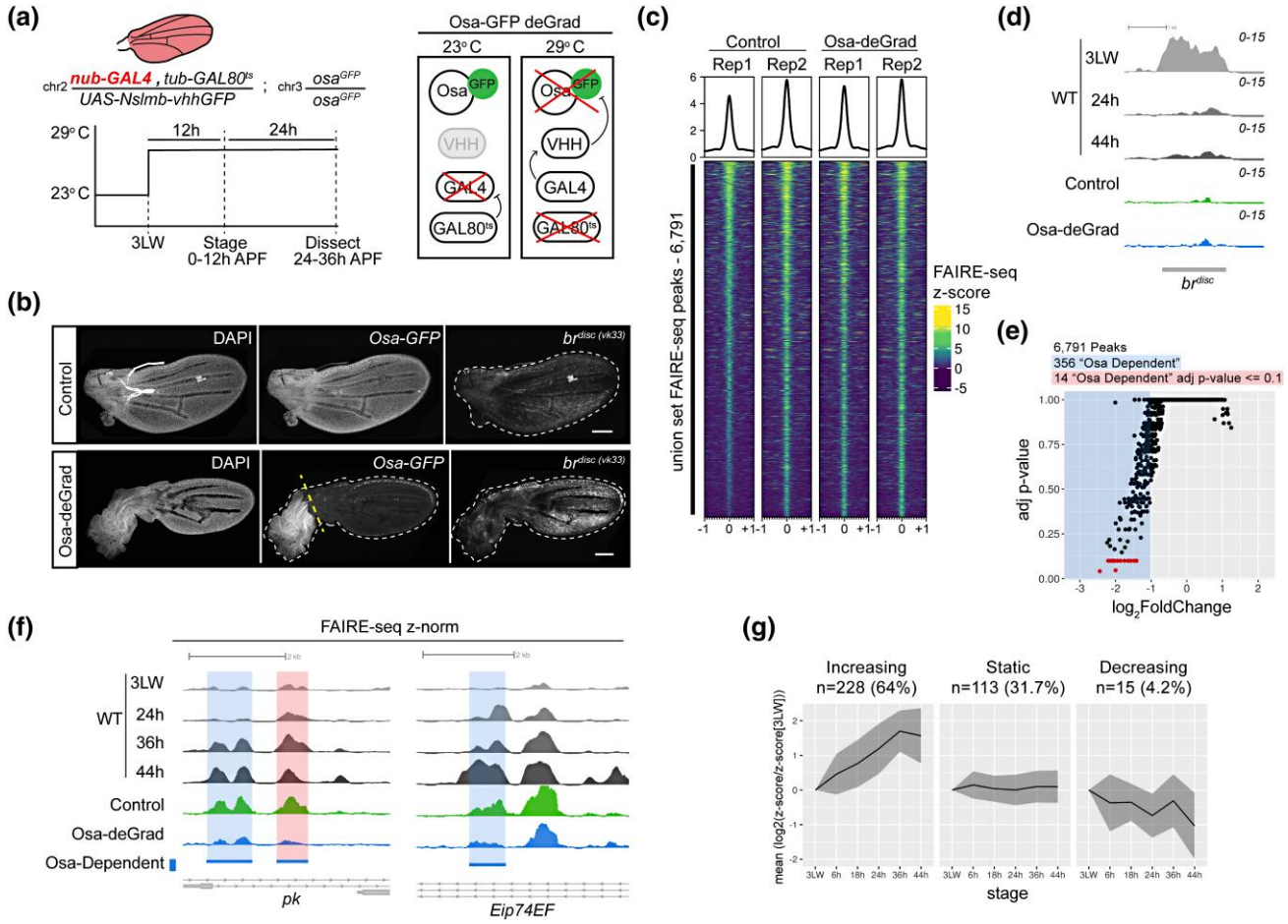

Fig. 3. Osa is not required to close br^{disc} and is dispensable for pupal chromatin accessibility patterns. a) Illustrations of osa^{GFP} degradation (Osa-deGrad) genotypes and experimental design using the *nub-GAL4* wing driver. Schematic of pupal wing highlights region of GFP degradation driven by the *nub-GAL4* driver (red). b) Confocal images of Osa-deGrad experimental genotypes. Yellow dashed line indicates where wings were cut during sample collection. Scale bars are 100 µm. Images are MIPs. c) Heatmaps and average signal plots of z-normalized FAIRE signal within the union set of FAIRE peaks from control and Osa-deGrad pupal wings. Plotted range is ±1 kb from peak center. Peaks are ranked by signal in control Rep1. d) Browser shot of z-normalized FAIRE signal from Osa-deGrad (blue), Osa-deGrad control (green), and WT (gray) imaginal wing discs at the endogenous br^{disc} enhancer. e) Scatterplot of $\log_2$FoldChange of Osa-deGrad/Control FAIRE-seq signal (x-axis) relative to adjusted *P*-value (y-axis). Peaks with $\log_2$FoldChange ≤ −1 (Osa-dependent) are highlighted in blue. Peaks with an adjusted $P \leq 0.1$ are colored red. f) Browser shot of FAIRE signal at representative "Osa-dependent" sites (blue bars and highlights, red highlight indicates adjusted $P < 0.1$) near the *prickle* (*pk*) and *Eip74EF* loci. g) Line plots of the average WT FAIRE $\log_2$FoldChange relative to 3LW, with standard deviation (SD) as gray ribbon, within 356 "Osa-dependent" sites. Sites are split by whether they increase in accessibility relative to the 3LW stage ("increasing"), have little change ("static"), or lose accessibility ("decreasing") (see Methods). The x-axis denotes stages of wing development from 3LW to 44 h APF. All z-normalized FAIRE signal in browser shots are pooled replicates.

Despite the strong impact of Osa-deGrad on wing development, br^{disc} reporter activity, and survival, FAIRE-seq revealed minimal changes in chromatin accessibility profiles relative to control samples, including at br^{disc} (Fig. 3c and d). A union set of 6,791 open chromatin peaks was identified between both control and Osa-deGrad samples (Supplementary Fig. 3d). Pearson correlation coefficients of z-normalized FAIRE signal revealed high correlation between both replicates of control and Osa-deGrad pupal wing profiles, indicating that Osa degradation minimally affects open chromatin profiles (Supplementary Fig. 3e). We conclude that increased br^{disc} activity observed in *osa* loss-of-function pupal wings is not due to failure to close the br^{disc} enhancer. These findings also demonstrate that developmentally programmed opening and closing of wing enhancers occur normally genome wide in the absence of Osa.

Previous studies in mammalian cells and *Drosophila* S2 cells have observed the role of Brahma complex orthologs in promoting chromatin accessibility (Kelso *et al.* 2017; Hendy *et al.* 2022; Hota *et al.* 2022). To test for the possibility of subtle changes in accessibility, we compared FAIRE signal between Osa-deGrad and control samples and observed a unidirectional skew toward lower FAIRE signal in Osa-deGrad relative to control (Fig. 3e). We note that while we find 356 regions (5.2%) with reduced accessibility ($\log_2$FoldChange ≤ −1, "Osa-dependent") following Osa-GFP degradation, only 14 (0.2% of all peaks) were found to be significantly different between conditions (adjusted $P \leq 0.1$) due to variability between replicates, raising the possibility that some of these regions are false positives. Examples of these Osa-dependent sites occurred at genes including *prickle* (*pk*) and the ecdysone response gene *Eip74EF* (Fig. 3f). Both of these Osa-dependent sites exhibit temporally dynamic accessibility, with low accessibility observed in larval wing imaginal discs becoming progressively more open later in pupal stages. To determine if temporally dynamic accessibility is a general feature of Osa-dependent FAIRE peaks, we categorized each peak as either "increased," "static," or "decreased" based on the WT FAIRE-seq signal at that site during pupal stages relative to the late larval stage (see Methods). We find that 64% (228/356) of

Osa-dependent sites correspond to regions that increase in accessibility between larval and pupal stages (Fig. 3g), whereas only 4.2% of Osa-dependent sites decrease in accessibility over the same time interval. This finding suggests that while the effect of Osa-GFP degradation is minor, the subtle losses in accessibility observed are most often associated with regions that open between the early and late wing development. Collectively, we conclude that Osa is not required for large, binary changes in "open" or "closed" chromatin over time during wing development. Instead, it is required for only a small number of sites to achieve full accessibility.

The br^{disc} reporter is active in a small number of pupal wing cells upon Osa loss of function

Our FAIRE-seq data indicate that Osa is not required for enhancer closing between the early and late stages of wing development. The finding that br^{disc} is closed in *osa* loss-of-function pupal wings raised the possibility that the enhancer is inactive despite the apparent increase in reporter activity. To directly test whether the br^{disc} enhancer is active in *osa* loss-of-function pupal wings, we utilized the dual-fluorophore br^{disc}-*switch* reporter (Fig. 1a). We first depleted Osa using the same RNAi-mediated knockdown conditions employed in the nucleosome remodeler screen, but we used the posterior *en-GAL4, tub-GAL80*^{ts} (*en*^{ts}) driver because the *ci-GAL4* driver contained a GFP marker that conflicted with the switch reporter. The switch from tdTomato to myr-GFP reporter output was induced at a time point after br^{disc} deactivation (>24 h APF). Under these conditions, we found that the enhancer remains inactive in the great majority of pupal wing cells, with a few notable exceptions. Whereas control lexA knockdown pupal wings exhibited nascent GFP along the margin and in the posterior crossvein, similar to the enhancer's pattern of activity in WT pupal wings (Fig. 1b), *osa* knockdown pupal wings also exhibited nascent GFP expression in a subset of cells in the wing blade (Fig. 4a). Notably, the membrane-localized myr-GFP of the br^{disc}-*switch* reporter revealed that wing blade cells in which br^{disc} was active exhibited a distinct morphology resembling shaft cells of adult sensory organs. These were similar in appearance to the shaft cells located along the wing margin in which the br^{disc} reporter normally reactivates during later pupal stages in WT animals (Fig. 4a, inset). Elevated levels of nascent GFP were also observed in the posterior margin of *osa* knockdown pupal wings (Fig. 4a). The detection of nascent GFP after br^{disc} normally closes and deactivates indicates that *osa* knockdown causes the enhancer to be inappropriately active in a small number of cells. However, br^{disc} activity was not detected in most cells that exhibited increased reporter levels in the initial nucleosome remodeler screen. It is possible that a small number of additional cells in which br^{disc} is active in *osa* knockdown pupal wings are too few to impact whole-wing open chromatin profiles, thus explaining the closed appearance of the enhancer in our FAIRE-seq data.

Sensory organs do not normally develop within the wing blade. In WT tissues, sensory organ precursors (SOPs) are specified with stereotypical spatial and temporal patterns, with the last SOPs in the wing being specified during prepupal stages. Once specified, SOPs undergo 2 rounds of cell division and fate specification, resulting in the development of a single shaft, socket, sheath, and neural cell, which together compose an adult sensory organ (Couso *et al.* 1994; Furman and Bukharina 2012). The appearance of br^{disc} activity in cells with shaft-like morphology in the wing blade indicates that *osa* knockdown leads to the development of ectopic sensory organs. Consistent with this hypothesis, *osa* knockdown also resulted in ectopic expression in the wing blade of Elav, a marker of neural cell identity (Supplementary Fig. 7). This finding is in agreement with prior studies in which combinations of *osa* hypomorphic alleles and loss-of-function clones caused ectopic sensory organ development (Heitzler *et al.* 2003; Terriente-Félix and de Celis 2009). We speculated that by initiating RNAi expression in larval wing discs, early loss of *osa* function leads to ectopic sensory organ development accompanied by br^{disc} activation. To test this hypothesis, we sought to knockdown *osa* function later in wing development, reasoning that the delay would reduce the likelihood of disrupting the development of sensory organs, which are determined by the end of prepupal stages (Couso *et al.* 1994). We returned to the Osa-deGrad system due to its rapid depletion of Osa protein, in combination with the *en*^{ts} driver. Osa degradation was initiated in 0- to 12-h prepupae, ~48 h later than initiation of knockdown in the RNAi screen. Examination of br^{disc} reporter activity 30 h later revealed 2 phenotypic classes that correlated with wing age. In younger pupal wings, there was clear derepression of br^{disc} in Osa-deGrad cells relative to WT cells in the same wing. By contrast, older pupal wings exhibited no sign of br^{disc} derepression in the wing blade (Fig. 4b). We interpret these findings as being a consequence of the developmental stage when Osa degradation was initiated. Since the duration of Osa depletion was the same for both phenotypic classes, the younger pupal wings, which exhibit br^{disc} derepression, would have been at an earlier developmental stage when Osa depletion was initiated than the older pupal wings, which do not exhibit br^{disc} derepression. We conclude that Osa is not required for br^{disc} deactivation. Instead, any detected increase in reporter activity is likely due to indirect consequences stemming from the disruption of *osa* function early in sensory organ development.

Osa is required to constrain br^{disc} reporter activity in wing imaginal discs

We hypothesized that if Osa and other BAP complex members are required for reduced br^{disc} reporter levels in pupal wings, as indicated by our RNAi screen results, but they are not required for chromatin closing or for br^{disc} reporter deactivation, then Osa may be required to repress br^{disc} reporter activity at an earlier stage of development (Fig. 2b). To test this hypothesis, we assayed br^{disc} reporter activity in wing imaginal discs following Osa knockdown, which corresponds to a developmental stage when br^{disc} is normally active. At this time point, wing discs are ~2 days younger than the pupal wings assayed in our RNAi screen. We observed a marked increase in reporter activity in *osa* knockdown cells relative to control cells. By contrast, a negative control RNAi targeting *lexA* did not affect br^{disc} reporter activity at this stage (Fig. 4c). Quantification of the ratio of reporter signal in RNAi-expressing vs control cells confirmed significant hyperactivation of the reporter in *osa* knockdown but not in control *lexA* knockdown cells ($P = 6.84e^{-14}$, 2-sample *t*-test; Fig. 4d). The requirement of the BAP complex to constrain br^{disc} activity in the wing disc was further validated by independent knockdown of a different BAP complex member *brm*, as well as an independent *osa* RNAi line (330350), both of which also resulted in increased br^{disc} reporter activity (Supplementary Fig. 4a). Thus, loss of Osa function results in hyperactivation of the br^{disc} enhancer in cells in which it is already active. Increased br^{disc} reporter levels following knockdown of BAP complex members indicate that BAP is required to constrain the activity of the enhancer in wing imaginal discs. Because we find no evidence that Osa is required to close the br^{disc} enhancer in pupal wings, we interpret the increased reporter activity observed in pupal wings to be a consequence of persistent reporter fluorophore following enhancer hyperactivation in wing imaginal discs (Fig. 2b, magenta line).

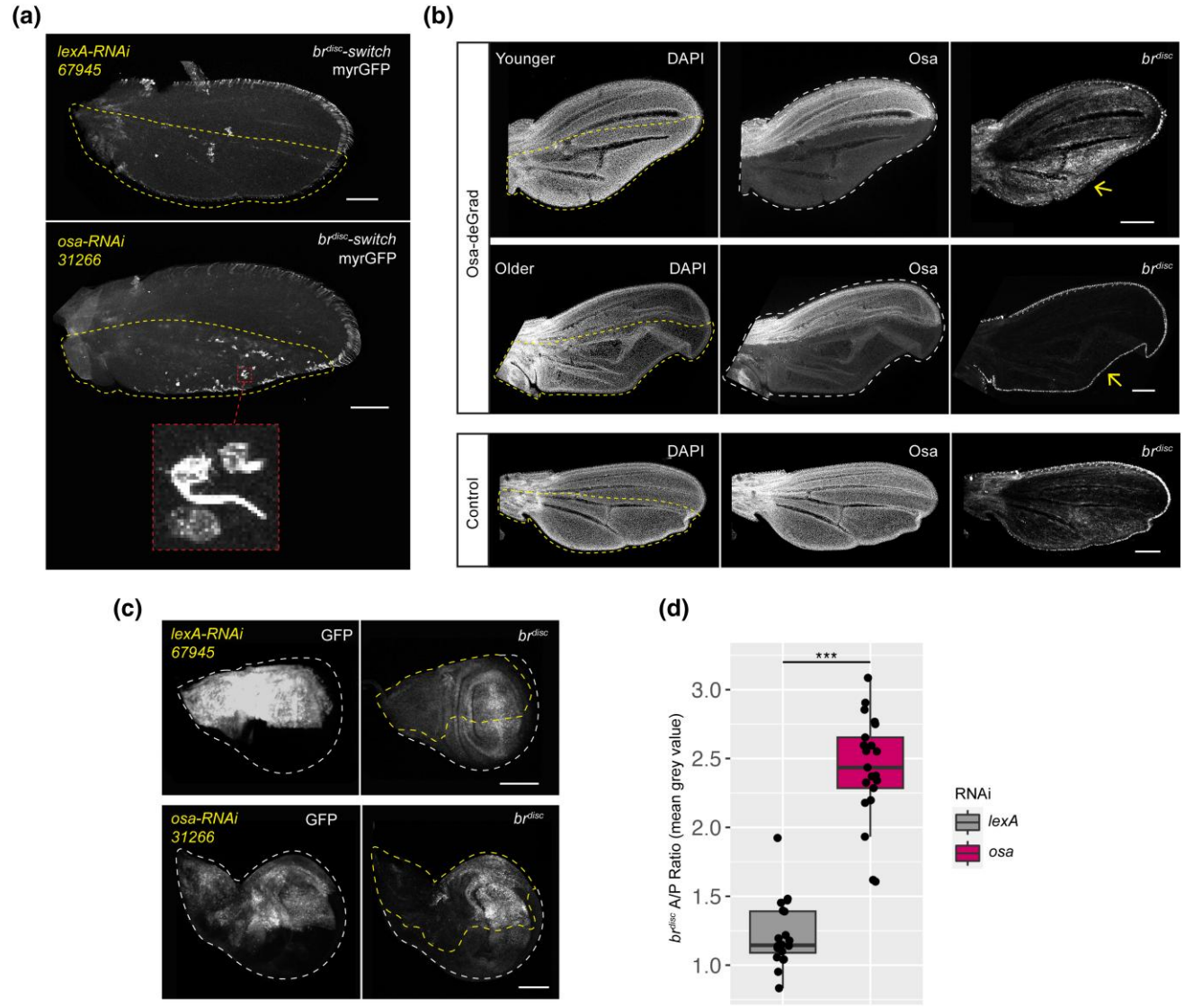

Fig. 4. Osa is required to constrain br^{disc} activity in wing imaginal discs. a) Confocal images of br^{disc}-*switch* nascent myr-GFP signal in the pupal wing in negative control *lexA* RNAi or *osa* RNAi. b) Confocal images of br^{disc}-*tdTomato-PEST* activity in 30–42 h APF wings following late induction of Osa-deGrad. Approximate regions of Osa degradation are outlined with yellow dashed line in the DAPI channel. "Younger" indicates a wing closer to 30 h APF of age. "Older" indicates a wing closer to 42 h APF (see Methods). A negative control in which Osa-deGrad was induced in an osa^{GFP} heterozygote (osa^{GFP}/*osa*) is shown for comparison (control). Yellow arrows denote regions of differential reporter activity for comparison. c) Confocal images of br^{disc} activity in *osa*-RNAi and control *lexA*-RNAi wing imaginal discs. GFP marks domain of RNAi expression (outlined by dashed yellow line). d) Quantification of br^{disc} reporter increase in response to *osa*-RNAi in wing imaginal discs, compared to control *lexA*-RNAi. The y-axis is a ratio of br^{disc} signal in the anterior (RNAi-expressing) vs the posterior (WT) cells. Asterisks indicate significance (***$P < 1e^{-13}$, 2-sample *t*-test). Images are MIPs. Scale bars are 100 µm.

Osa directly binds br^{disc} in larval wing imaginal discs as well as thousands of putative enhancers genome wide

Hyperactivation of the br^{disc} reporter in wing imaginal discs following degradation of BAP complex members could be due to a direct loss of BAP function at the enhancer or an indirect consequence of dysregulation of other br^{disc} inputs. To determine if the BAP complex directly binds br^{disc}, we performed CUT&RUN for Osa using the osa^{GFP} allele. We performed anti-GFP CUT&RUN in homozygous osa^{GFP} and WT control female wing imaginal discs. We identified 2,150 Osa-GFP peaks (see Methods), the great majority of which (1,953) did not overlap control peaks (Fig. 5a and b). We focused on this set of Osa-GFP-specific peaks ("Osa peaks") for all subsequent analyses.

Genomic feature annotation revealed that a majority of Osa peaks were enriched in distal intergenic regions and introns relative to a shuffled Osa peak control annotation (Fig. 5c). We found that Osa peaks were significantly more abundant in "introns" (48.6%, $P = 6.4e^{-58}$) and "5′ UTRs" (6.3%, $P = 7e^{-5}$). Osa peaks were significantly less abundant in "exons" (2.4%, $P = 5.7e^{-46}$) and "3′ UTRs" (0.8%, $P = 5e^{-35}$, 2-proportion z-test). Collectively, these findings indicate that Osa is predominantly bound to non-coding regions of the genome (86.6% promoter | distal intergenic | intron), consistent with an expected role in gene regulation. In order to focus our analysis on *cis*-regulatory elements with potential roles as developmentally dynamic enhancers, we selected Osa peaks that lie distal to promoters for use in subsequent analysis (1,358 peaks, "distal Osa peaks").

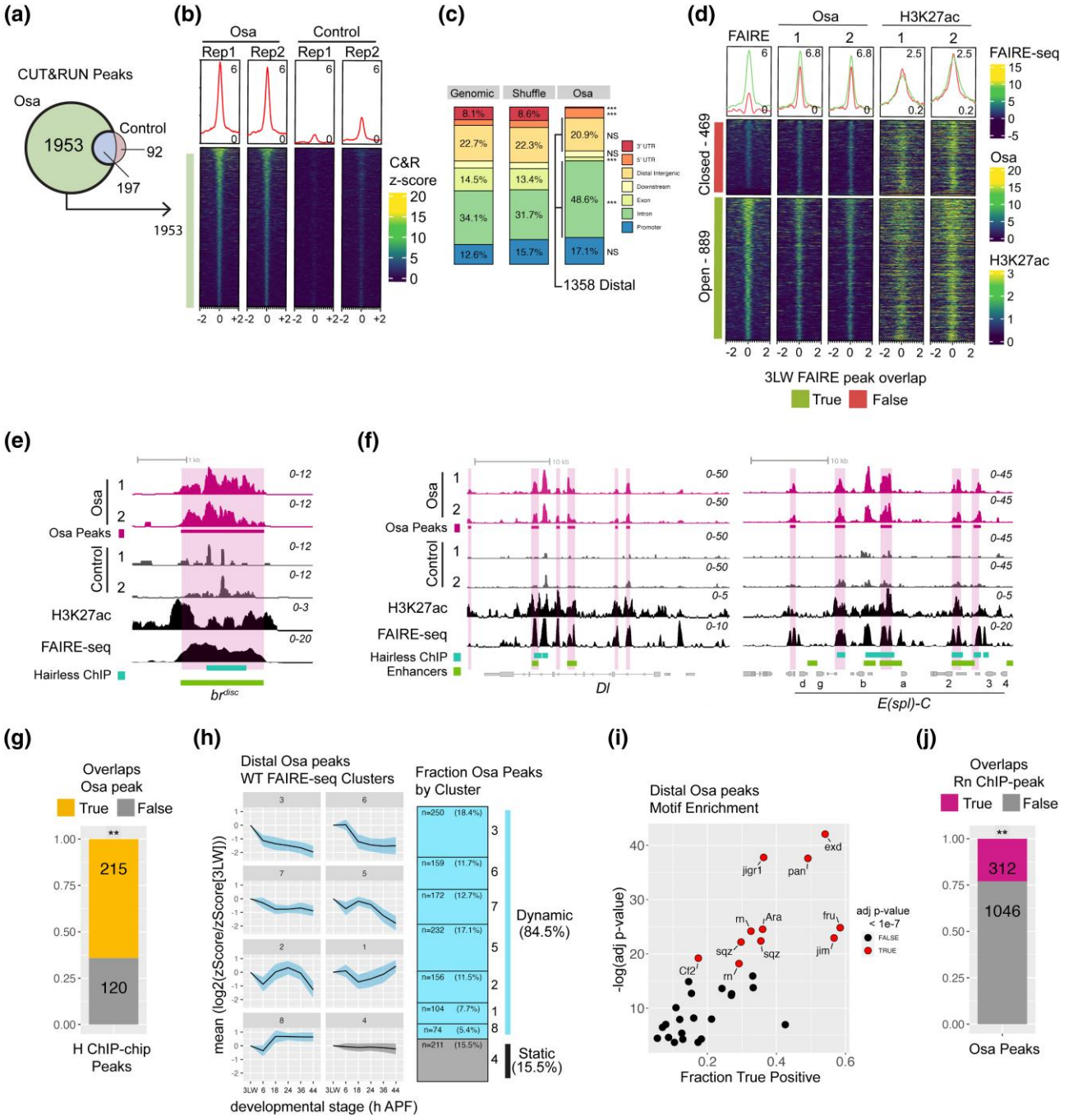

Fig. 5. Osa directly binds br^{disc} and thousands of putative enhancers in wing imaginal discs. a) Venn diagram of peaks called in Osa-GFP (Osa) vs control wing imaginal disc CUT&RUN experiments. b) Heatmap and average signal plots of z-normalized CUT&RUN signal between experimental replicates within Osa-specific peaks. c) Stacked bar plots of the distribution of Osa peak genomic annotations relative to a 500-bp tiled genome-wide annotation (genome), and a bootstrapped shuffle of Osa peaks (shuffle). Asterisks indicate significance (***$P < 0.0001$, 2-proportion z-test). d) Heatmap and average signal plots of wing imaginal disc z-normalized FAIRE-seq, Osa CUT&RUN, and H3K27ac CUT&RUN signal within distal Osa peaks. Heatmaps are grouped by whether Osa peaks overlap a FAIRE peak in 3LW wing discs. e, f) Browser shots of Osa CUT&RUN signal (magenta) vs control (gray), H3K27ac z-normalized signal (black), and WT FAIRE-seq (black). Coordinates for Osa peaks (magenta), Hairless ChIP peaks (teal), and annotated enhancers (green) are indicated. Browsers depict the br^{disc} enhancer e), and the *Dl* and *E(spl)-C* loci f). g) Bar plot showing fraction of Hairless ChIP peaks that overlap Osa peaks (not restricted to distal only). Asterisks indicate significance (**adjusted $P < 0.001$, permutation test). h) Line plots of the ratio of WT wing FAIRE-seq signal in distal Osa peaks for each of 6 developmental stages relative to 3LW (log_2). Osa peaks were placed into 8 categories by k-means clustering of the WT FAIRE time course data. SD shown by blue ribbon. Stacked bar plot depicts fraction of distal Osa peaks associated with each cluster. Dynamic clusters (1, 2, 3, 5, 6, 7, and 8) are colored blue. Static cluster (4) is colored gray. i) Scatterplot of motifs enriched in distal Osa peaks, plotted by –log(adjusted *P*-value) and fraction of true positive. Motifs with an adjusted $P < 1e^{-7}$ are colored in red. j) Bar plot of the fraction of distal Osa peaks that overlap Rn ChIP-seq peaks. Asterisks indicate significance (**adjusted $P < 0.001$, permutation test).

To evaluate the relationship between Osa binding and potential enhancer activity, we next examined the overlap between distal Osa peaks and open chromatin sites in wing imaginal discs (Uyehara *et al.* 2017). We found that most distal Osa peaks (65%, 889) were associated with a high degree of chromatin accessibility, whereas 35% (469) of distal Osa peaks did not overlap a FAIRE peak

in wing imaginal discs (Fig. 5d). Notably, 25% (119) of these Osa-bound "closed" sites were identified as a FAIRE peak in at least 1 later stage of wing development (Supplementary Fig. 5f). Thus, 74.2% (1008) of distal Osa peaks are bound at regions that are either open in wing imaginal discs or will open subsequently during a later stage of wing development. To further examine the regulatory potential of distal Osa peaks, we performed CUT&RUN for histone H3K27ac, an epigenetic mark associated with active enhancers, in wing imaginal discs. We found an enrichment of H3K27ac signal at highly accessible distal Osa peaks (Fig. 5d). Interestingly, we also found H3K27ac signal at distal Osa peaks that do not overlap a FAIRE peak, suggesting that some of these sites possess enhancer activity despite exhibiting low chromatin accessibility (Fig. 5d). Together, the correlation between chromatin accessibility and H3K27ac enrichment at distal Osa peaks indicates these sites are likely to function as enhancers in developing wings.

To further define the relationship between Osa occupancy and regulatory DNA, we examined binding at previously characterized enhancers. Firstly, we found that Osa is bound at the endogenous br^{disc} enhancer with broad signal observed across the entire enhancer in both replicates. By contrast, CUT&RUN signal apparent at the br^{disc} enhancer in control experiments was nonreproducible and restricted to narrow regions, which we interpret as being due to opportunistic MNase digestion of this highly accessible DNA (Fig. 5e). The presence of Osa at the endogenous br^{disc} enhancer strongly suggests that direct binding of the BAP complex to br^{disc} is required to constrain its activity.

In addition to br^{disc}, we observed Osa bound at multiple genes known to be regulated by the Brahma complex during wing development, such as at components of the Notch signaling pathway. There is a well-established connection between Brahma complexes and Notch signaling. Mutations in Notch pathway genes enhance *brm* dominant negative allele phenotypes, Osa loss of function increases expression of the proneural Notch targets *achaete* and *scute* (*ac/sc*), and both Brm and Mor are required for full induction of the Notch target genes in the *Enhancer of Split complex* (*E(spl)-C*) locus (Elfring *et al.* 1998; Heitzler *et al.* 2003; Armstrong *et al.* 2005; Pillidge and Bray 2019). Consistent with this relationship, we observed high-amplitude Osa binding sites at the genes encoding the Notch ligands *Delta* (*Dl*) and *Serrate* (ser), the Notch receptor *Notch* (*N*), and Notch target *E(spl)-C* genes (Fig. 5f; Supplementary Fig. 5a–c). At least two of the Osa peaks in the *Dl* locus correspond to previously characterized enhancers, including the Dl^{SOP} enhancer, which is active within SOP cells in wing imaginal discs, and the Dl^{teg} enhancer, which is active in the tegula, hinge, and anterior notum (Uyehara and McKay 2019). Osa binding in the *E(spl)-C* locus overlaps the mα, mβ, m2, and m3 enhancers, which contribute to proneural cluster development in wing imaginal discs. Like many signaling pathways, Notch signaling relies on the action of corepressors to limit the expression of Notch targets in the absence of a signal. In *Drosophila*, the corepressor Hairless binds the Notch signaling effector suppressor of Hairless (Su(H)) and has been found to bind hundreds of sites across the genome in the wing disc, including known regulatory sites that require Hairless for negative regulation (Chan *et al.* 2017). We found that the majority (64.2%) of Hairless peaks intersect with an Osa binding site, indicating a significant overlap between these gene regulatory proteins (adjusted $P = 9.99e^{-4}$, permutation test; Fig. 5g) and supporting the strong association between BAP complex function and Notch signaling. Hairless is also bound at the endogenous br^{disc} enhancer (Fig. 5e and f). To test the role of Notch signaling in br^{disc} regulation, we knocked down Hairless and Su(H) in wing imaginal discs. Expression of 2 independent RNAi lines targeting *Hairless* (*H*) and a third targeting Su(H) with the ci^{ts} driver caused lethality but did not affect br^{disc} activity (Supplementary Fig. 6a), arguing against a role for Notch in regulating br^{disc} activity.

In addition to binding known regulatory elements, we found that Osa binding is also correlated with genomic loci that exhibit temporal changes in chromatin accessibility. A previous FAIRE-seq time course of WT wings identified distinct patterns of temporal accessibility changes (Uyehara *et al.* 2017; Nystrom *et al.* 2020; Fig. 5h; Supplementary Fig. 5e). By clustering FAIRE signal in Osa-bound regulatory sites, we found that 84.5% of Osa-bound distal regulatory sites were associated with FAIRE-seq peaks that exhibited temporal changes during wing development, whereas only 15.5% of peaks exhibited static accessibility (Fig. 5h). The correlation between distal Osa peaks and dynamic rather than static accessibility indicates that Osa is associated with regulatory regions that are likely stage specific and are either being actively used at larval stages or possibly constrained from being used until a later stage.

Like most nucleosome remodeling complexes, the BAP complex does not exhibit sequence-specific DNA binding but is instead thought to be recruited to target loci by transcription factors. Osa contains an AT-rich interacting domain (ARID) that facilitates interaction with DNA, but this domain has been shown to confer little to no sequence preference on BAP complex DNA binding (Collins *et al.* 1999; Patsialou *et al.* 2005). To identify candidate factors that contribute to the recruitment of Osa to its binding sites, we performed motif enrichment analysis of sequences around distal Osa peaks. Of the highest significance motifs, several were associated with major signaling pathways and wing patterning programs. Notably, we found motifs for the homeodomain factors extradenticle and araucan, the wingless-signaling effector Pangolin (Pan), and the zinc-finger transcription factors squeeze and Rn (Fig. 5i). Examination of recently published Rn ChIP-seq data from wing imaginal discs revealed that 23% (312) of distal Osa peaks overlap with a Rn peak, which is greater than expected by chance as tested by overlap with shuffled Osa peak controls (adjusted $P = 9.99e^{-4}$, permutation test; Loker and Mann 2022; Fig. 5j). This correlation between Rn and Osa binding at regulatory sites in wing discs further supports the connection between Osa and active wing developmental programs. The observed enrichment of Pan motifs in Osa binding sites is also notable because Osa has been proposed to repress wingless target genes (Collins and Treisman 2000). Our findings indicate that this repression could be direct. For instance, the wingless target gene, *nubbin*, which is ectopically expressed in *osa* mutants, has several Osa binding sites in wing imaginal discs (Collins and Treisman 2000; Supplementary Fig. 5d). The enrichment of Pan motifs and others in Osa binding sites suggests that the BAP complex is broadly utilized by the major signaling pathways and patterning factors that shape wing development. Depletion of Pan by ci^{ts}-driven RNAi did not impact br^{disc} reporter activity despite causing notched wings and defects in notum morphology in adults, suggesting that Pan is not necessary for control of br^{disc} activity (Supplementary Fig. 6e).

A previous study demonstrated that components of the BAP and PBAP complexes bind the *Eip74EF* (*E74*) locus in larval salivary glands and that PBAP but not BAP is required for *E74* induction in response to ecdysone (Tilly *et al.* 2021). We observed multiple Osa binding sites within the *E74* locus in wing imaginal discs. Among the Osa-bound sites are 2 previously characterized wing disc enhancers, $E74^A$ and $E74^B$ (Uyehara *et al.* 2022). To test the potential role of Osa in regulating activity of these target enhancers in wing

discs, we depleted Osa via RNAi. Consistent with prior links between Brahma complex function and gene activation, we observed a loss in activity of both the $E74^{A}$ and the $E74^{B}$ enhancer upon Osa depletion (Supplementary Fig. 6c). Thus, Osa is required for the activation of 2 target enhancers in the same cells and at the same developmental time as it is required for constraint of the br^{disc} enhancer, indicating that Osa-dependent control of enhancer activity is locus specific. Notably, neither the $E74^{A}$ nor the $E74^{B}$ enhancer corresponds to the Osa-dependent open chromatin site identified by FAIRE at the *E74* locus in pupal wings, which is not bound by Osa in wing imaginal discs (Fig. 3f; Supplementary Fig. 6b). Consistent with this observation, we find that there is little correlation between patterns of Osa binding in larval wing imaginal discs and sites that depend on Osa to achieve full accessibility later in pupal wings: only 8% (30/356) of all potential Osa-dependent FAIRE peaks overlap a larval Osa binding site (Supplementary Fig. 6d). Collectively, the concerted presence of Osa binding at bona fide enhancers indicates that the BAP complex is a direct regulator of transcriptional programs with major roles in wing development.

Osa is required to constrain Delta activation in wing imaginal discs

Notch signaling performs multiple critical roles in wing imaginal discs. Notch-mediated lateral inhibition is necessary for selecting the SOP cells that form the chemosensory and mechanosensory organs of the adult wing. Notch signaling also initiates the specification of wing vein cell fates. Both of these processes depend on the patterned expression of the Notch ligand, *Dl*, which has an extensive *cis*-regulatory domain. It has been previously observed that Osa is involved in the regulation of *Dl* expression in parts of the wing disc pouch (Terriente-Félix and de Celis 2009). Due to the discovery of multiple Osa binding sites at known and putative enhancers within the *Dl* locus, we hypothesized that Osa regulates *Dl* expression directly. The *Dl* gene is expressed in third instar larval wing discs in 2 rows of cells flanking the dorsal–ventral (DV) boundary of the developing wing margin and in perpendicular stripes marking the developing veins (Doherty *et al.* 1996). In addition to the 2 previously characterized *Dl* enhancers described above, a third putative enhancer in the *Dl* locus was found to be highly accessible and to exhibit high levels of Osa CUT&RUN signal relative to nearby binding sites in wing imaginal discs (Fig. 6a). To test if this site functions as a transcriptional enhancer, we cloned it for transgenic reporter analysis. Two reporter versions were generated: one in which the enhancer was cloned upstream of GAL4 and a second in which the enhancer was cloned upstream of *tdTomato* with a C-terminal *PEST* degradation tag. Both reporters were active in a pattern overlapping *Dl* gene expression along the DV boundary and in the presumptive wing veins (Fig. 6b and c). Accordingly, we term this enhancer Dl^{pouch}. Using the Dl^{pouch}-*tdTomato-PEST* reporter and the ci^{ts} driver, we next tested the role of Osa in regulating Dl^{pouch} activity. We observed that Osa depletion resulted in increased enhancer activity relative to a *luciferase-RNAi* negative control (Fig. 6d). Quantification of Dl^{pouch} reporter signal, normalized to WT posterior cells (see Methods), revealed that Osa depletion caused enhancer hyperactivation ~2.5× above control levels ($P < 7e^{-11}$, 2-sample *t*-test; Fig. 6e). We conclude that Osa is necessary to directly constrain activity of this Dl enhancer, similar to its role in constraining br^{disc} enhancer activity. To determine whether the observed role of Osa in constraining activity of this transgenic reporter extended to endogenous *Dl* gene control, we performed immunofluorescence in Osa knockdown cells. Relative to *lexA* control RNAi, we find that depletion of Osa from the anterior compartment of the wing disc resulted in increased Dl levels and subtle expansion of the Dl pattern most notably around the L2 provein stripe, similar to the effect of Osa depletion on the Dl^{pouch} enhancer (Fig. 6f). Quantification revealed that Dl levels were significantly higher in Osa knockdown relative to control ($P < 9e^{-11}$, 2-sample *t*-test; Fig. 6g). Together, these findings demonstrate that enhancer hyperactivation in the absence of the BAP complex is correlated with increased expression of the Notch ligand.

Discussion

We set out to investigate the possible roles of nucleosome remodeling complexes in developmentally programmed enhancer regulation, with a particular focus on enhancer closing and deactivation. Using reporters of the previously characterized and developmentally dynamic wing enhancer, br^{disc}, we performed an in vivo RNAi screen that identified members of the *Drosophila* SWI/SNF (BAP) complex as repressors of enhancer activity. Surprisingly, we find that the BAP-specific subunit Osa is not required to close br^{disc} and is globally dispensable for binary changes in accessibility, closing or opening, between the early and late stages of wing development (Fig. 3). Rather than being required for enhancer deactivation, we instead find that Osa is required to constrain the activity of the br^{disc} enhancer when it is in the ON state in wing discs (Fig. 4). Genome-wide profiling revealed that Osa binds extensively to sites with signatures of active regulatory DNA (open and H3K27ac enriched), including at multiple known and putative enhancers of Notch pathway component genes (Fig. 5). Comparison of DNA binding profiles of Osa and the Notch corepressor Hairless revealed significant coenrichment of these proteins genome wide, suggesting a direct coregulatory relationship between Notch signaling responses and the BAP complex. Finally, although we found that Osa is required to activate enhancers from the *E74* gene, we also determined that Osa depletion leads to hyperactivation of a newly reported *Dl* enhancer and upregulation of Delta protein. Together, these findings support a central role of Osa and the BAP complex in regulating Notch pathway activity, and they suggest a general role for Osa in controlling the magnitude of gene expression through the constraint of enhancer activation (Fig. 6).

Is the BAP complex required for control of chromatin accessibility in developing *Drosophila* wings?

Thousands of *cis*-regulatory elements exhibit chromatin accessibility changes during the first 2 days of pupal wing development in *Drosophila*, which drive the dynamic gene expression changes that underlie the progressive determination of cell fates (Uyehara *et al.* 2017; Ma *et al.* 2019). We hypothesized that nucleosome remodeling complexes work with sequence-specific transcription factors to bring about these kilobase-sized transitions in chromatin state. However, we observed no requirement for Osa in either opening or closing enhancers genome-wide (Fig. 3). This is a surprising finding because SWI/SNF complex function has been found to be required for proper control of chromatin accessibility in both mammalian and *Drosophila* cells. For example, in *Drosophila* S2 cells, degradation of the core SWI/SNF subunit Snr1 was found to lead to significant loss of accessibility at developmental enhancers but not at promoters or housekeeping enhancers (Hendy *et al.* 2022). In mammalian systems, genetic removal or chemical inhibition of the SWI/SNF ATPase Brg1 in mouse embryonic stem cells results in loss of accessibility

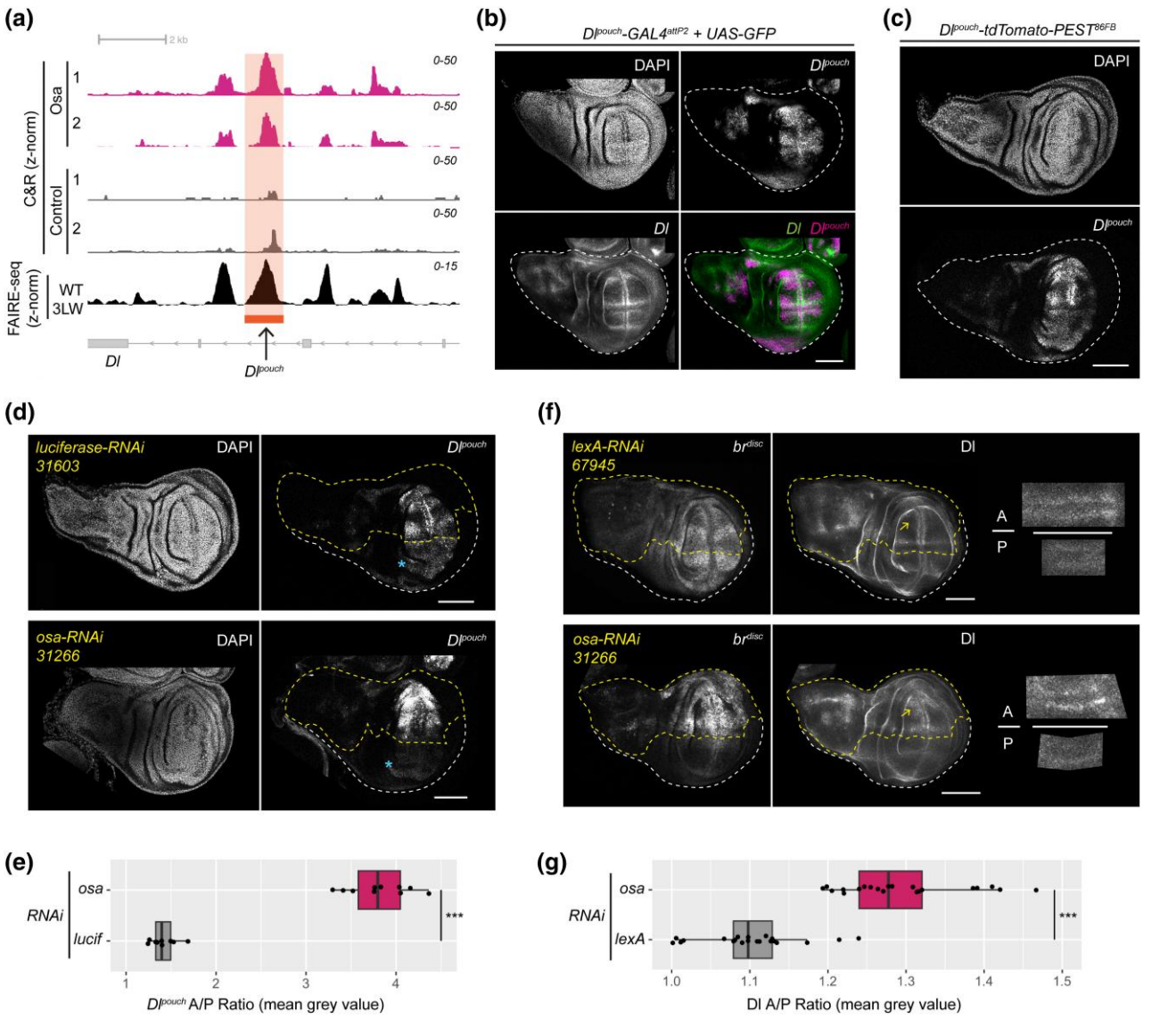

Fig. 6. Osa negatively regulates Delta expression. a) Genome browser shot of the *Dl* locus with Osa-GFP and control CUT&RUN (C&R) replicates, and WT 3LW wing disc FAIRE-seq. All tracks are z-normalized. The Dl^{pouch} enhancer is highlighted in orange. b) Confocal images of the Dl^{pouch}-GAL4 reporter in combination with a *UAS-GFP* in WT wing imaginal discs stained for Dl protein. c) Confocal images of the Dl^{pouch}-*tdTomato-PEST*^{86FB} reporter in WT wing imaginal discs, and d) in the context of either *osa-RNAi or* control *luciferase-RNAi* expression. Note that image acquisition was optimized to limit pixel saturation, causing the levels of enhancer activity in WT (posterior) cells to appear lower in the *luciferase-RNAi* condition relative to the *osa-RNAi* condition (blue asterisks). e) Quantification of Dl^{pouch} levels in *osa-RNAi* vs *luciferase-RNAi* control experiments, with signal in the anterior normalized to WT cells of the posterior in the same wing. f) Confocal images (max intensity projection) of br^{disc} reporter activity and immunofluorescence of Delta protein in wing imaginal discs from negative control *lexA* or *osa* RNAi. Insets show representative ROI selections in the anterior ("A") and posterior ("P") compartments used for quantification (see Methods). Yellow arrows highlight expansion of Dl pattern around L2 provein relative to control. g) Image quantification of Delta levels in *lexA* control and *osa* RNAi experiments. Asterisks indicate significance (***$P < 1e^{-10}$, 2-sample *t*-test). RNAi-expressing cells are outlined with yellow dashed line. Images are single z-slices unless otherwise noted. Scale bars are 100 µm.

genome wide (Iurlaro et al. 2021). Similarly, loss of the Osa ortholog ARID1A, which is commonly mutated in cancers (Kadoch *et al.* 2013), results in both loss and gain of open chromatin sites in human cells (Kelso *et al.* 2017). SWI/SNF has also been shown to be required during mammalian developmental programs. $Brm^{-/-}$ null mouse embryonic stem cells fail to establish normal patterns of chromatin accessibility during cardiomyocyte differentiation, which is correlated with a widespread dysregulation of gene expression including activation of noncardiomyocyte lineage gene programs (Hota *et al.* 2022). Whereas we observed subtle decreases in accessibility at a subset of open chromatin sites upon Osa knockdown, we did not find evidence for a global role of Osa in binary chromatin state transitions from closed to open or open to closed during pupal wing development. It is unlikely that the lack of an open chromatin phenotype is due to insufficient sensitivity of the experimental approach because the same assay (FAIRE-seq) was used previously in pupal wings to detect large-scale changes in chromatin accessibility following depletion of the ecdysone-induced transcription factor E93 (Uyehara *et al.* 2017). For these reasons, we conclude that Osa is not globally required for developmentally programmed changes to open chromatin profiles in pupal wings. An alternative explanation is that our methods did not sufficiently deplete Osa below a minimal threshold. We disfavor this possibility because no Osa-GFP signal

remains after nanobody-mediated degradation, and immunostaining with Osa antibodies likewise revealed little nuclear signal above background (Supplementary Fig. 3). Moreover, we observed developmental phenotypes consistent with Osa loss of function. Another possible explanation is that the role of the BAP complex in regulating chromatin accessibility is compensated for by the PBAP complex. Synthetic lethal phenotypes caused by perturbation of subunits from distinct SWI/SNF complex subtypes have been reported, supporting the potential of functional redundancy (Helming *et al.* 2014; Wilson *et al.* 2014; Michel *et al.* 2018). Lastly, multiple nucleosome remodelers can be found at the same genomic targets (Morris *et al.* 2014), raising the possibility of compensation by other complexes.

What is enhancer constraint?

SWI/SNF nucleosome remodeling complexes were first identified for their role in counteracting Polycomb-mediated repression and establishing regions of nucleosome depletion in order to facilitate transcription (Kassis *et al.* 2017; Cenik and Shilatifard 2021). Subsequent work has demonstrated that SWI/SNF complexes are required to maintain nucleosome-depleted regions, high levels of H3K27ac, and enrichment of the histone variant H3.3 at enhancers and promoters (Alver *et al.* 2017; Blümli *et al.* 2021; Schick *et al.* 2021; Weber *et al.* 2021; Hendy *et al.* 2022; Reske *et al.* 2022). In addition to their role in gene activation, SWI/SNF complexes have also been implicated in gene repression (Treisman *et al.* 1997; Moshkin *et al.* 2007; Zraly and Dingwall 2012; Kelso *et al.* 2017; Weber *et al.* 2021), including repression of wingless target genes during wing development (Collins and Treisman 2000). Here, we find that the BAP complex constrains the activity of the developmentally dynamic br^{disc} enhancer, but it is not required for closing or deactivation. DNA binding profiles reveal that Osa binds the br^{disc} enhancer while it is active in developing imaginal wing discs, suggesting its role in enhancer constraint is direct. We discovered a similar role for Osa in preventing hyperactivation of the newly described Dl^{pouch} enhancer and the *Dl* gene itself. How might SWI/SNF function to achieve constraint? SWI/SNF complexes are generally understood to slide and/or eject nucleosomes by translocating DNA around the histone octamer (Clapier *et al.* 2017). Nucleosome mobilization could result in repression if DNA translocation blocked a binding site for an activator. Conversely, increased accessibility mediated by SWI/SNF could uncover a repressor binding site. Differential accessibility of repressor binding sites in a wing spot enhancer was recently proposed as a mechanism involved in morphological diversification between *Drosophila* species (Ling *et al.* 2023). Another possible direct mechanism is through changes in histone acetylation via collaboration with the NuRD complex. A recent study in human endometriotic epithelial cells demonstrated that the Osa ortholog ARID1A is required to maintain levels of the histone variant H3.3 at active enhancers, which in turn is required to recruit NuRD complex components and limit the accumulation of H3K27ac levels (Reske *et al.* 2022). Lastly, iterative cycles of nucleosome remodeling activity driven by ATP hydrolysis could impact the dynamics of transcription factor occupancy at target enhancers, which in turn could impact their potency as transcriptional regulators (Morris *et al.* 2014; Brahma and Henikoff 2023). In addition to these direct mechanisms, it is also possible, though not mutually exclusive, that SWI/SNF-dependent enhancer constraint is an indirect consequence of SWI/SNF-dependent repressor activation. For example, failure to activate the transcriptional repressors encoded by the *Enhancer of split complex* locus could contribute to hyperactivation of Notch pathway target genes in *Osa* loss of function wings (see below).

The BAP complex as a direct regulator of Notch signaling

Our findings point to an important role of Osa in Notch pathway function. This is supported by prior studies that have discovered strong regulatory connections between the Notch pathway and the BAP complex. Genetic screens found that alleles of *Dl* dominantly enhance phenotypes of an ATP-ase dead *brm* allele (brm^{K804R}; Armstrong *et al.* 2005). BAP complex members have also been found to regulate the expression of Notch signaling targets, such as genes encoded by the *Enhancer of split complex* and *achaete/scute* loci (Armstrong *et al.* 2005; Pillidge and Bray 2019). Our genomic profiling of Osa in wing imaginal discs revealed clusters of Osa binding at putative regulatory sites at loci encoding the Notch ligands Dl and Ser, at the gene encoding the *Notch* receptor itself, and at enhancers of the *Enhancer of split complex* (Fig. 5; Supplementary Fig. 5). Interestingly, it has been previously reported that Osa negatively regulates expression of the proneural genes *achaete* and *scute*, but we observed little binding of Osa around these genes sparing a single potential binding site that also has a relatively high degree of signal in negative controls (Armstrong *et al.* 2005). This suggests the regulation of *achaete* and *scute* by the BAP complex may be indirect. In addition to the extensive binding of Osa at genes encoding Notch pathway components, we also find significant coenrichment of Osa binding and the Notch pathway corepressor Hairless, including at the br^{disc} enhancer (Fig. 5g). Thus, the BAP complex may directly regulate Notch target genes genome wide. Together, our binding data strengthen the previously observed regulatory relationship between the BAP complex and Notch signaling.

Several observations made through the course of our study suggest a regulatory connection between the br^{disc} enhancer, the BAP complex, and the Notch signaling pathway. Although we find that depletion of the Notch transcriptional regulators Hairless and Su(H) does not impact br^{disc} activity, the enhancer may still be responsive to Notch pathway input. The pattern of br^{disc} activity in wing imaginal discs suggests positive input from Notch signaling. The highest levels of enhancer activity in the pouch of wing imaginal discs are typically observed along the presumptive wing margin and in 2 DV stripes that extend away from the margin that resembles the wing proveins (Fig. 4c). Each of these regions overlaps high levels of Dl expression. The activity of br^{disc} in pupal wings is also suggestive of Notch pathway input. Br^{disc} is reactivated in the sensory organs located along the wing margin in late-stage WT pupal wings. Notch signaling is required for determining the fates of these sensory organ cells. Moreover, sensory organ development is particularly sensitive to the levels of Notch pathway signaling, with too much or too little Notch signaling leading to sensory organ developmental defects. Hyperactivation of the Notch pathway may also explain the development of ectopic sensory organs and activation of the br^{disc} enhancer in shaft cells of the developing pupal wing blade upon Osa loss of function. Collectively, these observations suggest that the br^{disc} enhancer is responsive to Notch signaling and that the BAP complex may be required to directly constrain Notch target gene activity. A lack of proper constraint by the BAP complex at enhancers of Notch signaling component genes and of Notch target genes may result in the observed development of ectopic bristles and neurons (Supplementary Fig. 7). This possibility is further supported by our observation that Osa is required to prevent hyperactivation of the Dl^{pouch} enhancer and the *Dl* gene itself

(Fig. 6). We note that prior studies describe a role of Osa in activation of *Dl* in wing imaginal discs, which contrasts with our observations (Terriente-Félix and de Celis 2009). We attribute this discrepancy as being due to the different spatial patterns and timing of the GAL4 drivers used. Altogether, our data support a direct role for the BAP nucleosome remodeling complex in mediating the proper levels of Notch pathway signaling during wing development.

Data availability

Strains and plasmids are available upon request. High-throughput sequencing data are publicly available online at GEO (GSE244556). Code used to process sequencing data and generate plots can be found at https://github.com/mniederhuber/Niederhuber_2023.

Supplemental material available at GENETICS online.

Acknowledgments

The authors thank Christopher Uyehara and Kale Hartmann for help generating the Dl^{pouch} reporter constructs and Spencer Nystrom for writing the FAIRE-seq and CUT&RUN pipelines and some of the R utility functions used for analysis. Antibodies obtained from DSHB, created by the NICHD of the NIH, are maintained by the University of Iowa, Department of Biology, Iowa City, IA, 52242. Stocks obtained from the Bloomington Drosophila Stock Center (NIH P40OD018537) were used in this study. Additional transgenic fly stocks were obtained from the Vienna Drosophila Resource Center (VDRC, *www.vdrc.at*).

Funding

This work was supported by the National Institute of General Medical Sciences (NIGMS) grant R35GM128851 to DJM. MJN was supported in part by NIGMS Grant T32GM007092 and by National Science Foundation Graduate Research Fellowship Award Number 1650116.

Conflicts of interest

The author(s) declare no conflicts of interest.

Literature cited

Alver BH, Kim KH, Lu P, Wang X, Manchester HE, Wang W, Haswell JR, Park PJ, Roberts CWM. 2017. The SWI/SNF chromatin remodelling complex is required for maintenance of lineage specific enhancers. Nat Commun. 8(1):16468. doi:10.1038/ncomms14648.

Amemiya HM, Kundaje A, Boyle AP. 2019. The ENCODE blacklist: identification of problematic regions of the genome. Sci Rep. 9(1):9354. doi:10.1038/s41598-019-45839-z.

Armstrong JA, Sperling AS, Deuring R, Manning L, Moseley SL, Papoulas O, Piatek CI, Doe CQ, Tamkun JW. 2005. Genetic screens for enhancers of brahma reveal functional interactions between the BRM chromatin-remodeling complex and the Delta–Notch signal transduction pathway in *Drosophila*. Genetics. 170(4): 1761–1774. doi:10.1534/genetics.105.041327.

Bhardwaj V, Heyne S, Sikora K, Rabbani L, Rauer M, Kilpert F, Richter AS, Ryan DP, Manke T. 2019. Snakepipes: facilitating flexible, scalable and integrative epigenomic analysis. Bioinformatics. 35(22):4757–4759. doi:10.1093/bioinformatics/btz436.

Blümli S, Wiechens N, Wu M-Y, Singh V, Gierlinski M, Schweikert G, Gilbert N, Naughton C, Sundaramoorthy R, Varghese J, *et al.* 2021. Acute depletion of the ARID1A subunit of SWI/SNF complexes reveals distinct pathways for activation and repression of transcription. Cell Rep. 37(5):109943. doi:10.1016/j.celrep.2021.109943.

Bouazoune K, Brehm A. 2006. ATP-dependent chromatin remodeling complexes in *Drosophila*. Chromosome Res. 14(4):433–449. doi:10.1007/s10577-006-1067-0.

Brahma S, Henikoff S. 2020. Epigenome regulation by dynamic nucleosome unwrapping. Trends Biochem Sci. 45(1):13–26. doi:10.1016/j.tibs.2019.09.003.

Brahma S, Henikoff S. 2023. RNA Polymerase II, the BAF remodeler and transcription factors synergize to evict nucleosomes. bioRxiv 2023.01.22.525083. https://doi.org/10.1101/2023.01.22.525083.

Buszczak M, Paterno S, Lighthouse D, Bachman J, Planck J, Owen S, Skora AD, Nystul TG, Ohlstein B, Allen A, *et al.* 2007. The carnegie protein trap library: a versatile tool for *Drosophila* developmental studies. Genetics. 175(3):1505–1531. doi:10.1534/genetics.106.065961.

Caussinus E, Kanca O, Affolter M. 2012. Fluorescent fusion protein knockout mediated by anti-GFP nanobody. Nat Struct Mol Biol. 19(1):117–121. doi:10.1038/nsmb.2180.

Cenik BK, Shilatifard A. 2021. COMPASS And SWI/SNF complexes in development and disease. Nat Rev Genet. 22(1):38–58. doi:10.1038/s41576-020-0278-0.

Chan SKK, Cerda-Moya G, Stojnic R, Millen K, Fischer B, Fexova S, Skalska L, Gomez-Lamarca M, Pillidge Z, Russell S, *et al.* 2017. Role of co-repressor genomic landscapes in shaping the notch response. PLoS Genet. 13(11):e1007096. doi:10.1371/journal.pgen.1007096.

Cho B, Song S, Axelrod JD. 2020. Prickle isoforms determine handedness of helical morphogenesis. eLife. 9:e51456. doi:10.7554/eLife.51456.

Clapier CR, Iwasa J, Cairns BR, Peterson CL. 2017. Mechanisms of action and regulation of ATP-dependent chromatin-remodelling complexes. Nat Rev Mol Cell Biol. 18(7):407–422. doi:10.1038/nrm.2017.26.

Collins RT, Furukawa T, Tanese N, Treisman JE. 1999. Osa associates with the brahma chromatin remodeling complex and promotes the activation of some target genes. EMBO J. 18(24):7029–7040. doi:10.1093/emboj/18.24.7029.

Collins RT, Treisman JE. 2000. Osa-containing Brahma chromatin remodeling complexes are required for the repression of wingless target genes. Genes Dev. 14(24):3140–3152. doi:10.1101/gad.854300.

Couso JP, Bishop SA, Martinez Arias A. 1994. The wingless signalling pathway and the patterning of the wing margin in *Drosophila*. Development. 120(3):621–636. doi:10.1242/dev.120.3.621.

Danecek P, Bonfield JK, Liddle J, Marshall J, Ohan V, Pollard MO, Whitwham A, Keane T, McCarthy SA, Davies RM, *et al.* 2021. Twelve years of SAMtools and BCFtools. Gigascience. 10(2): giab008. doi:10.1093/gigascience/giab008.

Diaz de la Loza MC, Thompson BJ. 2017. Forces shaping the *Drosophila* wing. Mech Dev. 144:23–32. doi:10.1016/j.mod.2016.10.003.

Doherty D, Feger G, Younger-Shepherd S, Jan LY, Jan YN. 1996. Delta is a ventral to dorsal signal complementary to serrate, another Notch ligand, in *Drosophila* wing formation. Genes Dev. 10(4): 421–434. doi:10.1101/gad.10.4.421.

Elfring LK, Daniel C, Papoulas O, Deuring R, Sarte M, Moseley S, Beek SJ, Waldrip WR, Daubresse G, DePace A, *et al.* 1998. Genetic analysis of brahma: the *Drosophila* homolog of the yeast chromatin

remodeling factor SWI2/SNF2. Genetics. 148(1):251–265. doi:10.1093/genetics/148.1.251.

Falo-Sanjuan J, Bray SJ. 2020. Decoding the Notch signal. Dev Growth Differ. 62(1):4–14. doi:10.1111/dgd.12644.

Furman DP, Bukharina TA. 2012. Morphogenesis of *Drosophila* melanogaster macrochaetes: cell fate determination for bristle organ. J Stem Cells. 7(1):19–41.

Gaskill MM, Gibson TJ, Larson ED, Harrison MM. 2021. GAF is essential for zygotic genome activation and chromatin accessibility in the early *Drosophila* embryo. eLife. 10:e66668. doi:10.7554/eLife.66668.

Gramates LS, Agapite J, Attrill H, Calvi BR, Crosby MA, Santos Dos, Goodman G, Goutte-Gattat JL, Jenkins D, Kaufman VK. 2022. FlyBase: a guided tour of highlighted features. Genetics. 220(4). doi:10.1093/genetics/iyac035.

Gu Z, Eils R, Schlesner M. 2016. Complex heatmaps reveal patterns and correlations in multidimensional genomic data. Bioinformatics. 32(18):2847–2849. doi:10.1093/bioinformatics/btw313.

Guild GM, Connelly PS, Ruggiero L, Vranich KA, Tilney LG. 2005. Actin filament bundles in *Drosophila* wing hairs: hairs and bristles use different strategies for assembly. Mol Biol Cell. 16(8):3620–3631. doi:10.1091/mbc.E05-03-0185.

Hahne F, Ivanek R. 2016. Visualizing genomic data using Gviz and bioconductor. In: Mathé E, Davis S, editors. Statistical Genomics: Methods and Protocols. New York (NY): Springer. p. 335–351.

Hartenstein V, Posakony JW. 1990. A dual function of the Notch gene in *Drosophila* sensillum development. Dev Biol. 142(1):13–30. doi:10.1016/0012-1606(90)90147-b.

Heitzler P, Vanolst L, Biryukova I, Ramain P. 2003. Enhancer-promoter communication mediated by Chip during Pannier-driven proneural patterning is regulated by Osa. Genes Dev. 17(5):591–596. doi:10.1101/gad.255703.

Helming KC, Wang X, Wilson BG, Vazquez F, Haswell JR, Manchester HE, Kim Y, Kryukov GV, Ghandi M, Aguirre AJ, *et al.* 2014. ARID1B is a specific vulnerability in ARID1A-mutant cancers. Nat Med. 20(3):251–254. doi:10.1038/nm.3480.

Hendy O, Serebreni L, Bergauer K, Muerdter F, Huber L, Nemčko F, Stark A. 2022. Developmental and housekeeping transcriptional programs in *Drosophila* require distinct chromatin remodelers. Mol Cell. 82(19):3598–3612.e7. doi:10.1016/j.molcel.2022.08.019.

Hota SK, Rao KS, Blair AP, Khalilimeybodi A, Hu KM, Thomas R, So K, Kameswaran V, Xu J, Polacco BJ, *et al.* 2022. Brahma safeguards canalization of cardiac mesoderm differentiation. Nature. 602(7895):129–134. doi:10.1038/s41586-021-04336-y.

Isbel L, Grand RS, Schübeler D. 2022. Generating specificity in genome regulation through transcription factor sensitivity to chromatin. Nat Rev Genet. 23(12):728–740. doi:10.1038/s41576-022-00512-6.

Iurlaro M, Stadler MB, Masoni F, Jagani Z, Galli GG, Schübeler D. 2021. Mammalian SWI/SNF continuously restores local accessibility to chromatin. Nat Genet. 53(3):279–287. doi:10.1038/s41588-020-00768-w.

Kadoch C, Hargreaves DC, Hodges C, Elias L, Ho L, Ranish J, Crabtree GR. 2013. Proteomic and bioinformatic analysis of mammalian SWI/SNF complexes identifies extensive roles in human malignancy. Nat Genet. 45(6):592–601. doi:10.1038/ng.2628.

Kassis JA, Kennison JA, Tamkun JW. 2017. Polycomb and trithorax group genes in *Drosophila*. Genetics. 206(4):1699–1725. doi:10.1534/genetics.115.185116.

Kelso TWR, Porter DK, Amaral ML, Shokhirev MN, Benner C, Hargreaves DC. 2017. Chromatin accessibility underlies synthetic lethality of SWI/SNF subunits in ARID1A-mutant cancers. eLife. 6:1–29. doi:10.7554/eLife.30506.001.

Langmead B, Salzberg SL. 2012. Fast gapped-read alignment with Bowtie 2. Nat Methods. 9(4):357–359. doi:10.1038/nmeth.1923.

Li X, Zhao X, Fang Y, Jiang X, Duong T, Fan C, Huang CC, Kain SR. 1998. Generation of destabilized green fluorescent protein as a transcription reporter. J Biol Chem. 273(52):34970–34975. doi:10.1074/jbc.273.52.34970.

Ling L, Mühling B, Jaenichen R, Gompel N. 2023. Increased chromatin accessibility promotes the evolution of a transcriptional silencer in *Drosophila*. Sci Adv. 9(7):eade6529. doi:10.1126/sciadv.ade6529.

Loker R, Mann RS. 2022. Divergent expression of paralogous genes by modification of shared enhancer activity through a promoter-proximal silencer. Curr Biol. 32(16):3545–3555.e4. doi:10.1016/j.cub.2022.06.069.

Love MI, Huber W, Anders S. 2014. Moderated estimation of fold change and dispersion for RNA-seq data with DESeq2. Genome Biol. 15(12):550. doi:10.1186/s13059-014-0550-8.

Ma Y, McKay DJ, Buttitta L. 2019. Changes in chromatin accessibility ensure robust cell cycle exit in terminally differentiated cells. PLoS Biol. 17(9):e3000378. doi:10.1371/journal.pbio.3000378.

Mallo M, Alonso CR. 2013. The regulation of Hox gene expression during animal development. Development. 140(19):3951–3963. doi:10.1242/dev.068346.

McLeay RC, Bailey TL. 2010. Motif enrichment analysis: a unified framework and an evaluation on ChIP data. BMC Bioinformatics. 11(1):165. doi:10.1186/1471-2105-11-165.

Michel BC, D'Avino AR, Cassel SH, Mashtalir N, McKenzie ZM, McBride MJ, Valencia AM, Zhou Q, Bocker M, Soares LMM, *et al.* 2018. A non-canonical SWI/SNF complex is a synthetic lethal target in cancers driven by BAF complex perturbation. Nat Cell Biol. 20(12):1410–1420. doi:10.1038/s41556-018-0221-1.

Millán-Zambrano G, Burton A, Bannister AJ, Schneider R. 2022. Histone post-translational modifications—cause and consequence of genome function. Nat Rev Genet. 23(9):563–580. doi:10.1038/s41576-022-00468-7.

Morris SA, Baek S, Sung M-H, John S, Wiench M, Johnson TA, Schiltz RL, Hager GL. 2014. Overlapping chromatin-remodeling systems collaborate genome wide at dynamic chromatin transitions. Nat Struct Mol Biol. 21(1):73–81. doi:10.1038/nsmb.2718.

Moshkin YM, Mohrmann L, van Ijcken WFJ, Verrijzer CP. 2007. Functional differentiation of SWI/SNF remodelers in transcription and cell cycle control. Mol Cell Biol. 27(2):651–661. doi:10.1128/MCB.01257-06.

Mu W, Davis ES, Lee S, Dozmorov MG, Phanstiel DH, Love MI. 2023. Bootranges: flexible generation of null sets of genomic ranges for hypothesis testing. Bioinformatics. 39(5):btad190. doi:10.1093/bioinformatics/btad190.

Nern A, Pfeiffer BD, Svoboda K, Rubin GM. 2011. Multiple new site-specific recombinases for use in manipulating animal genomes. Proc Natl Acad Sci. 108(34):14198–14203. doi:10.1073/pnas.1111704108.

Niederhuber MJ, McKay DJ. 2021. Mechanisms underlying the control of dynamic regulatory element activity and chromatin accessibility during metamorphosis. Curr Opin Insect Sci. 43:21–28. doi:10.1016/j.cois.2020.08.007.

Nystrom SL, McKay DJ. 2021. Memes: a motif analysis environment in R using tools from the MEME suite. PLoS Comput Biol. 17(9):e1008991. doi:10.1371/journal.pcbi.1008991.

Nystrom SL, Niederhuber MJ, McKay DJ. 2020. Expression of E93 provides an instructive cue to control dynamic enhancer activity and chromatin accessibility during development. Development. 147(6):dev181909. doi:10.1242/dev.181909.

Parks AL, Muskavitch MA. 1993. Delta function is required for bristle organ determination and morphogenesis in *Drosophila*. Dev Biol. 157(2):484–496. doi:10.1006/dbio.1993.1151.

Patsialou A, Wilsker D, Moran E. 2005. DNA-binding properties of ARID family proteins. Nucleic Acids Res. 33(1):66–80. doi:10.1093/nar/gki145.

Pillidge Z, Bray SJ. 2019. SWI/SNF chromatin remodeling controls Notch-responsive enhancer accessibility. EMBO Rep. 20(5): e46944. doi:10.15252/embr.201846944.

Ramírez F, Ryan DP, Grüning B, Bhardwaj V, Kilpert F, Richter AS, Heyne S, Dündar F, Manke T. 2016. deepTools2: a next generation web server for deep-sequencing data analysis. Nucleic Acids Res. 44(W1):W160–W165. doi:10.1093/nar/gkw257.

Reske JJ, Wilson MR, Armistead B, Harkins S, Perez C, Hrit J, Adams M, Rothbart SB, Missmer SA, Fazleabas AT, *et al.* 2022. ARID1A-dependent Maintenance of H3.3 is required for repressive CHD4-ZMYND8 chromatin interactions at super-enhancers. BMC Biol. 20(1):209. doi:10.1186/s12915-022-01407-y.

Salzler HR, Vandadi V, McMichael BD, Brown JC, Boerma SA, Leatham-Jensen MP, Adams KM, Meers MP, Simon JM, Duronio RJ, *et al.* 2023. Distinct roles for canonical and variant histone H3 lysine-36 in Polycomb silencing. Sci Adv. 9(9):eadf2451. doi:10.1126/sciadv.adf2451.

Schick S, Grosche S, Kohl KE, Drpic D, Jaeger MG, Marella NC, Imrichova H, Lin JMG, Hofstätter G, Schuster M, *et al.* 2021. Acute BAF perturbation causes immediate changes in chromatin accessibility. Nat Genet. 53(3):269–278. doi:10.1038/s41588-021-00777-3.

Schindelin J, Arganda-Carreras I, Frise E, Kaynig V, Longair M, Pietzsch T, Preibisch S, Rueden C, Saalfeld S, Schmid B, *et al.* 2012. Fiji: an open-source platform for biological-image analysis. Nat Methods. 9(7):676–682. doi:10.1038/nmeth.2019.

Sobala LF, Adler PN. 2016. The gene expression program for the formation of wing cuticle in *Drosophila*. PLoS Genet. 12(5):e1006100. doi:10.1371/journal.pgen.1006100.

Spitz F, Furlong EEM. 2012. Transcription factors: from enhancer binding to developmental control. Nat Rev Genet. 13(9):613–626. doi:10.1038/nrg3207.

Stark R, Brown G. 2011. DiffBind: differential binding analysis of ChIP-seq peak data. Bioconductor. http://bioconductor.org/packages/release/bioc/html/DiffBind.html.

Tang Y-C, Amon A. 2013. Gene copy-number alterations: a cost-benefit analysis. Cell. 152(3):394–405. doi:10.1016/j.cell.2012.11.043.

Terriente-Félix A, de Celis JF. 2009. Osa, a subunit of the BAP chromatin-remodelling complex, participates in the regulation of gene expression in response to EGFR signalling in the *Drosophila* wing. Dev Biol. 329(2):350–361. doi:10.1016/j.ydbio.2009.03.010.

Tilly BC, Chalkley GE, van der Knaap JA, Moshkin YM, Kan TW, Dekkers DH, Demmers JA, Verrijzer PC. 2021. In vivo analysis reveals that ATP-hydrolysis couples remodeling to SWI/SNF release from chromatin. eLife. 10:e69424. doi:10.7554/eLife.69424.

Treisman JE, Luk A, Rubin GM, Heberlein U. 1997. Eyelid antagonizes wingless signaling during *Drosophila* development and has homology to the bright family of DNA-binding proteins. Genes Dev. 11(15):1949–1962. doi:10.1101/gad.11.15.1949.

Uyehara CM, Apostolou E. 2023. 3D enhancer-promoter interactions and multi-connected hubs: organizational principles and functional roles. Cell Rep. 42(4):112068. doi:10.1016/j.celrep.2023.112068.

Uyehara CM, Leatham-Jensen M, McKay DJ. 2022. Opportunistic binding of EcR to open chromatin drives tissue-specific developmental responses. Proc Natl Acad Sci. 119(40). doi:10.1073/pnas.2208935119.

Uyehara CM, McKay DJ. 2019. Direct and widespread role for the nuclear receptor EcR in mediating the response to ecdysone in *Drosophila*. Proc Natl Acad Sci. 116(20):9893–9902. doi:10.1073/pnas.1900343116.

Uyehara CM, Nystrom SL, Niederhuber MJ, Leatham-Jensen M, Ma Y, Buttitta LA, McKay DJ. 2017. Hormone-dependent control of developmental timing through regulation of chromatin accessibility. Genes Dev. 31(9):862–875. doi:10.1101/gad.298182.117.

Weber CM, Hafner A, Kirkland JG, Braun SMG, Stanton BZ, Boettiger AN, Crabtree GR. 2021. mSWI/SNF promotes Polycomb repression both directly and through genome-wide redistribution. Nat Struct Mol Biol. 28(6):501–511. doi:10.1038/s41594-021-00604-7.

Wickham H. 2016. ggplot2: Elegant Graphics for Data Analysis. New York (NY): Springer-Verlag.

Wilson BG, Helming KC, Wang X, Kim Y, Vazquez F, Jagani Z, Hahn WC, Roberts CWM. 2014. Residual complexes containing SMARCA2 (BRM) underlie the oncogenic drive of SMARCA4 (BRG1) mutation. Mol Cell Biol. 34(6):1136–1144. doi:10.1128/MCB.01372-13.

Yamanaka N, Rewitz KF, O'Connor MB. 2013. Ecdysone control of developmental transitions: lessons from *Drosophila* research. Annu Rev Entomol. 58(1):497–516. doi:10.1146/annurev-ento-120811-153608.

Yu G, Wang L-G, He Q-Y. 2015. ChIPseeker: an R/Bioconductor package for ChIP peak annotation, comparison and visualization. Bioinformatics. 31(14):2382–2383. doi:10.1093/bioinformatics/btv145.

Zhang Y, Liu T, Meyer CA, Eeckhoute J, Johnson DS, Bernstein BE, Nusbaum C, Myers RM, Brown M, Li W, *et al.* 2008. Model-based analysis of ChIP-Seq (MACS). Genome Biol. 9(9):R137. doi:10.1186/gb-2008-9-9-r137.

Zraly CB, Dingwall AK. 2012. The chromatin remodeling and mRNA splicing functions of the Brahma (SWI/SNF) complex are mediated by the SNR1/SNF5 regulatory subunit. Nucleic Acids Res. 40(13):5975–5987. doi:10.1093/nar/gks288.

Editor: P. Geyer